

HOW TO ASSESS UNFROZEN WATER CONTENT USING
CAPACITANCE SENSORS IN FROZEN SOILS: A NEW PHYSICS
BASED CONVERSION CURVE - MASC THESIS

by

QUENTIN "QUINN" SAPIN

A thesis submitted to the
Graduate Program of Civil Engineering
in conformity with the requirements for
the degree of Master of Applied Science

Queen's University
Kingston, Ontario, Canada
August 2025

Copyright © Quentin "Quinn" Sapin, 2025

Abstract

Over the past 50 years, the effects of anthropogenic climate change has lead to steady global warming. Despite the alarming rate at which our planet is experiencing those environmental disturbances, the scientific community has only just begun to understand and catalog their impact. Among the most impacted systems are polar and sub-polar regions which are warming at up to four times the average global rate, resulting in permafrost thaw. The amount of unfrozen water in soils governs their thermal, physical and chemical properties, and the rapid decay of permafrost around the globe has led to a resurgence in interest for accurate and reliable measurements of unfrozen water content in soils. This measurement is hard to acquire because most (if not all) existing measurement techniques are indirect. That is, another property/value is measured and is used as an indication of the amount of unfrozen water in the soil. Accordingly, there is a need for what is called a conversion curve: a relationship that can transform the measured raw data into the desired unfrozen water content values. Regardless of the precision and accuracy of the measurement apparatus, if the conversion curve is lacking, so are the data reported. Among current measurement techniques, capacitance based sensors are frequently used for both field and laboratory application because of their low cost and ease of installation and maintenance. The current conversion curve used in those sensors is the *Topp, 1980* equation, an empirical third-degree polynomial fit obtained from pooled wetting-drying experimental data. The *Topp* relation

is empirically fitted to entirely unfrozen data, resulting in a *Topp, 1980* equation that is not intended for use on frozen soil data. The goal of this paper is to present an alternative conversion curve for capacitance-based sensors using a multiphase dielectric mixing model that is physically grounded. This improves the mathematical conversion of field and laboratory dielectric permittivity measurements into an estimate of volumetric water content.

Co-Authorship

Quentin "Quinn" Sapin is the sole author of this thesis. This work was conducted under the supervision of professor Élise Devoie as a MSc thesis in the Civil Engineering Department at Queen's University. Chapter 3 of this thesis has been written as a scientific paper which will be submitted to Vadose Zone Journal or a different scientific journal shortly after the graduation of Quinn in September, 2025. Professor Devoie has provided comments and suggestions on both the content and style of writing for the paper and the entire thesis. Dr. Devoie is a co-author of the publication (Chapter 3).

Acknowledgments

Queen’s University is situated on the territory of the Haudenosaunee Confederacy and Anishinaabek Nation. I am honoured and grateful to live, learn and play with diligence on these lands. I am always learning to tread lightly and with careful respect because the histories of these lands are sacred and merit honour.

Ne Queen’s University e’tho nón:we nikanónhsote tsi nón:we ne Haudenosaunee táhnon Anishinaabek tehatihsnonhsáhere ne onhwéntsya. Gimaakwe Gchi-gkinoomaagegamiig atemagad Naadowe miinwaa Anishinaabe aking.

I would like to thank my parents and PSAC901 for the monetary support that allowed me to complete my graduate studies here at Queen’s University. Without them, it would have been absolutely unsustainable to do so. I would also like to thank my supervisor professor Élise Devoie for all the wonderful research opportunities she enabled me to engage with during my stay under her mentorship. They truly have shaped my early career as a young scientist. I would also like to thank Dr. da Silva for her work as head of the Civil Engineering department and for her support and guidance during my stay at Queen’s. Special shoutout to bun purse, my everyday rabbit supporter. Thanks to Frankee (@Frankee_makes_things) for creating her and providing me with amazing pieces of clothes.

I would like to acknowledge that the Queen's administration has failed to divest from interests which funded the persecution of the people of Palestine during the invasion of Palestine by the Israeli state. I strongly condemn the violence and genocidal war waged by Israel on the people of Palestine.

During my stay at Queen's University from the Summer of 2023 to the Summer of 2025, I have experienced many of the shortcomings of the current state of the Academic System. During the PSAC 901 Strike that occurred from March 10th to April 17th 2025, as a graduate student I felt intimidated and persecuted through legal means by bylaw enforcement, Kingston police enforcement, private investigators, and private security personnel on campus while I was exercising my right to protest. I perceived unwillingness displayed by members of the Queen's administration at the bargaining table, showing little regard for the well-being of the graduate population. This has been reflected in the contract ratified on April 17th. Queen's University presents itself as a modern, progressive and lgbtq+ inclusive university, but has failed to make an unambiguous statement against the anti-lgbtq+ and anti-trans protests that occurred in the Summer of 2023 and 2024. The Summer of 2023 was also marked by the inclusion of anti-lgbtq+ remarks in a final examination, which were publicly endorsed by Jordan Peterson, a known traditionalist and polarizing figure. I felt that Queen's failed to comment to the general public condemning this behaviour. Queen's university has supported me as a trans individual and nearly every single person I have interacted with at Queen's has shown respect for my gender identity. Queen's administration allowed me to use my preferred pronouns (she\they) and have my name be displayed as: "Quentin Quinn Sapin" on my diploma and transcript, which I greatly appreciate.

Author's Note

" I'd rather make enlightened choices about something [soil parameters] that might be wrong rather than none at all."

Quentin "Quinn" S., ICOP 2024, Whitehorse, Yukon, Kwanlin Dün Cultural Centre, June 2024. Second Poster Session.

List of Abbreviations and symbols

A_s Specific Surface Area in m^2/g

Å Angstroms in 10^{10} m

C Specific Heat Capacity

CNT Classical Nucleation Theory

δ Thickness of the Layer of Strongly Bounded Water in Angstroms [\AA]

∂ Partial Derivative

Δ Delta or "Change/Difference"

DI Deionized [water]

ε Dielectric Permittivity

ε_{eff}, ε_{apparent} Effective/Apparent Dielectric Permittivity

ε_{i,n} Dielectric Permittivity of the nth Inclusion (See Sihvola (2000))

ε₁ Dielectric Permittivity of Free Water

ε₂ Dielectric Permittivity of Bound Water

ϵ_{mix} , ϵ_w Dielectric Permittivity of Water Phase

i Imaginary Number i.e. $\sqrt{-1}$

i.e. "id est," or "in other words"

$Im(\mathbb{Z})$ Imaginary Domain

FID Free-Induction Decay

G Gibbs Free Energy in joules

J Work in joules

m Meters

MHz Mega Hertz (10^6 Hz)

NMR Nuclear Magnetic Resonance

OM Organic Matter

θ Volumetric Water Content

θ_{uwc} , θ_{water} , θ_{res} Volumetric Unfrozen Water Content

θ_{sbw} Strongly Bounded Volumetric Water Content

$^{\circ}C$ Degree Celsius

ϕ Porosity

\mathbb{R} Real Domain

ρ_b Soil Bulk Density [g/cm^3]

r Ice Crystal Radius

r^* Critical Ice Critical Radius

SLS Solid–Liquid-Solid Contact Soil

SS Solid–Solid Contact Soil

SSA Specific Surface Area

SWCC Soil Wetting Characteristic Curve

SFCC Soil Freezing Characteristic Curve

t Time

T Temperature in $^{\circ}\text{C}$

T_2 Relaxation Times (Fourier Transform Spectrum)

T_i First Major Trigger of Ice Nucleation (Temeprature)

T_f Bulk Melting Point (Temperature)

TDR Time Domain Reflectometry

V Volume

ν/ν Volumetric Ratio

Contents

Abstract	i
Co-Authorship	iii
Acknowledgments	iv
Author's Note	vi
List of Abbreviations and symbols	vii
Contents	x
List of Tables	xii
List of Figures	xiii
Chapter 1: Introduction	1
1.1 Goals and Research Question	4
Chapter 2: Literature Review	5
2.1 Cold Regions Warming	5
2.2 The Physics of Soil Freezing Processes	8
2.2.1 Unfrozen Water Content: Soil Freezing Characteristic Curves (SFCCs)	8
2.2.2 Nucleation of Ice	10
2.3 Estimate of θ_{uwc} : SWCC to SFCC	15
2.4 Hysteresis	18
2.5 Measurement of θ_{uwc} : Instrumentation	20
2.5.1 Field Measurement Techniques	21
2.5.2 Lab Measurement Techniques	23
2.6 Conversion Curves: From measurement to Ice content	25
2.6.1 The Current Conversion Curve: The Problem with <i>Topp, 1980</i>	26
2.6.2 Dielectric Mixing Models	27

2.6.3 Other Models	29
Chapter 3: How to Assess Unfrozen Water Content Using Capacitance Sensors in Frozen Soils: A New Physics Based Conversion Curve	31
3.1 Introduction	32
3.2 Methods	36
3.2.1 Fully Saturated 3 Phase Mixing Model	37
3.2.2 Volume Correction for Expansion of Ice	39
3.2.3 Adaptive Dielectric of Water Phase	40
3.2.4 Strongly Bound Water Characterization	41
3.3 Experimental Method	42
3.4 Results	44
3.5 Discussion	46
3.5.1 Error in parameter estimation	47
3.5.2 Sensitivity to parameter selection	48
3.5.3 Comparison with Topp	49
3.5.4 Impact of under-estimating unfrozen water content in freezing soils	50
3.5.5 Sources of error	52
3.5.6 Limitations in the applicability of the conversion curve	54
3.6 Conclusion	56
3.7 Data Availability	56
Chapter 4: Conclusions and Recommendations	57
4.1 Conclusions	57
4.2 Contributions	59
4.3 Limitations and Recommendations	60
Bibliography	62
Appendix A: Time Program Analysis and Temperature Correction	77
Appendix B: Solver	83
Appendix C: Raw Dielectric Permittivity Data Example	86

List of Tables

3.1	Description of the 6 soils used for Freeze-Thaw experiments, the source of water used, and the change in residual volumetric water content based on the choice of conversion curve. The silica flour has a mean volume size of 60 μm . Extra metadata about each soil which is necessary to use the mixing model can be found in Appendix B, Table B.1.	46
B.1	: Input parameters for the 6 soils used for Freeze-Thaw experiments. These are required to run the model presented in Figure B.1.	84

List of Figures

1.1	Representation of a case study soil sample as a randomly distributed multi-phase heterogeneous system of soil grains, air, unfrozen, frozen and bound water.	3
2.1	Permafrost temperature trend from 1975 to 2016 from Biskaborn et al. (2019).	7
2.2	Idealized representation of a Soil Freezing Characteristic Curve modified from Devoie et al. (2022).	9
2.3	The activation energy barrier and its relationship to the radius r of a crystal nucleating in a medium from Maeda (2021).	12
2.4	Depiction of the connection between SFCCs (left) and hysteresis (right). The SFCC on the left side does not encompass any temporal dependence, despite its "raw data" being time dependent. The hysteresis is apparent once the time dependence t is shown/kept (right). Time t_1 and t_2 are "reversal points" where the freeze-thaw direction of the temperature evolution in the system is reversed.	19
2.5	Theoretical scanning Curves for a hysteretic system from Bertotti and Mayorgoyz (2014). Notice the dotted scanning curve which approaches the main hysteretic curve asymptotically before reconnecting to the main hysteretic loop at x^*	20

3.1	Idealized representation of a Soil Freezing Characteristic Curve modified from Devoie et al. (2022)	33
3.2	Schematic representation of a soil sample in cryotic conditions. The Sihvola Multiphase Mix Model can be adapted to represent the soil sample in an environment, e , of liquid water in which the other phases exist. Note that while ice and air phases are not depicted as round for ease of visualization, they are only mathematically represented as such.	38
3.3	Theoretical representation of $\varepsilon_{water} = f(\theta_{water}, T)$, the temperature dependence reported in equation 3.7 (Malmberg and Maryott, 1956) is applied for above-zero temperatures (right), and for $T < 0^{\circ}CC$, equation 3.6 is applied (left). This is an example of synthetic data from a soil that would have porosity $\phi = 0.28 (v/v)$ and $\theta_{sbw} = 0.02$	42
3.4	Comparison of volumetric unfrozen water content (θ_{uwc}) data for two soils. Both the <i>Topp, 1980</i> conversion curve (\bullet) and the multiphase dielectric model (*) developed in this paper are represented. The coloured arrows indicate the direction of the freeze to thaw cycle direction for clarity, where the freezing limb has greater unfrozen water content than the thawing limb for equivalent temperatures.	44
3.5	Complete dataset of 6 soil types and 8 Freeze-Thaw programs. Both the <i>Topp, 1980</i> conversion curve (\bullet) and the multiphase dielectric model (\blacklozenge) developed in this paper are represented.	45
3.6	Sensitivity analysis on input parameters for the same dataset presented in Figure 3.4. Both the <i>Topp, 1980</i> conversion curve (\bullet) and the multiphase dielectric model (*) developed in this paper are represented.	47

A.1	Experimental Time Program for a fully saturated bucket of 20/30 sand. Notice the significant time (x axis) and temperature (y axis) lag between the blue (Temperature sensor reading) and green (Time Program) data points showing, respectively, the heat propagation into the bucket and the response of the sensor. The red (raw dielectric permittivity) data points are to be used as a proxy to illustrate the progressive formation of ice in the system.	78
A.2	Time Program for a fully saturated 800 ml beaker of silica sand. Notice the consistent offset from the sensor's temperature (in blue) and the climate chamber's time program (in green).	79
A.3	Residuals (in black) of the sensor's Temperature VS the Time Program for a fully saturated 800 ml beaker of silica sand.	80
A.4	Corrected Temperature VS the Time Program for a fully saturated 800 ml beaker of silica sand.	81
A.5	Residual study for Equilibrium points selection.	82
A.6	Final Data set of Equilibrium Points to be converted with the Conversion Curve.	82
B.1	Schematic representation of the iterative solver for the system of equations describing the mixing model developed in this study. The system of equations comprises Eq. 3.5, Eq. 3.6 and Eq. 3.8.	83

Chapter 1

Introduction

In the face of unprecedented climate warming, permafrost has been decaying worldwide (Biskaborn et al., 2019). For the past 50 years, global surface temperatures have steadily and increasingly climbed, exceeding conservative forecasts and temperature models (Rantanen et al., 2022; Wan et al., 2022). These major disturbances have caused disruptions to planetary systems, such as permafrost temperature, the impact of which have just begun to be understood and cataloged (Walvoord and Kurylyk, 2016; Lemieux et al., 2024).

The unfrozen water content of permafrost governs its thermal-hydro-mechanical properties (Jin et al., 2022, 2021; Fisher et al., 2019; Kleinberg and Griffin, 2005; Watanabe and Osada, 2017). To reliably and accurately measure the unfrozen water content in cryotic soil is crucial to tackle the rapid changes that northern regions are undergoing (Rantanen et al., 2022). These environmentally driven changes affect both natural environments and infrastructures, and accurately estimating unfrozen water content has become a growing priority for policy makers, researchers, engineers and inhabitants of permafrost rich regions.

There are several techniques currently used to assess unfrozen water content in cryotic soils,

each with their own merits and shortcomings (Devoie et al., 2022). This thesis has a focus on the capacitance-based method, a measurement technique which uses the dielectric permittivity of media to gain insight into their composition. In other words: the dielectric permittivity of soils differs depending on their water content, which can be interpreted to estimate their unfrozen water content (METER, 2025b; Evans, 1965; Malmberg and Maryott, 1956). This measurement technique requires the transformation of effective dielectric permittivity ϵ_{eff} into volumetric unfrozen water content θ_{uwc} using a conversion curve. The most widely used conversion curve for the capacitance measurement method is the *Topp, 1980* equation, a third degree empirical fit of wetting and drying curves that has been extended into the frozen domain (Topp et al., 1980; METER, 2025a). The author of this thesis argues that the *Topp, 1980* model is inadequate for this application in the cryotic domain because it i) uniformizes behavior on soils that are largely physically distinct from one another, ii) lacks any connection to ice crystal nucleation or phase change of water, iii) uses empirical fitting parameters that are unrelated to the soil sample characteristics and iv) has been extended beyond the temperature domain it was designed to be used on i.e. $< 0^{\circ}\text{C}$.

According to Sihvola, the dielectric permittivity of a three-phase system can be represented by Equation 1.1:

$$\epsilon_{eff} = \epsilon_e + 3\epsilon_e \frac{\sum_{n=1}^N \theta_n \frac{\epsilon_n - \epsilon_e}{\epsilon_n + 2\epsilon_e}}{1 - \sum_{n=1}^N \theta_n \frac{\epsilon_n - \epsilon_e}{\epsilon_n + 2\epsilon_e}} \quad (1.1)$$

where θ_n is the volume fraction of the inclusions of the n th phase in the environment e and ϵ_n is the dielectric permittivity of the inclusion. Though not present in current literature, this model can be translated to a three-phase system including soil-water-ice following similar logic to that presented in Sihvola. According to Sihvola *et al.*: "[...]To write down

the mixing rule for mixtures where there are several components, one has to choose one of the components as the host and then treat the polarization effect of all of the guest phases separately [...] (Sihvola, 2000). For cryotic soils, the system is broken down into its components, as seen in Figure 1.1 and characterized in terms of θ_n i.e. the volumetric fraction of each component {1, 2...n} in the system, yielding:

$$\theta_{total} \equiv 1 \equiv \theta_1 + \theta_2 + \dots \theta_n \quad (1.2)$$

for any medium with n number of phases (See Figure 1.1).

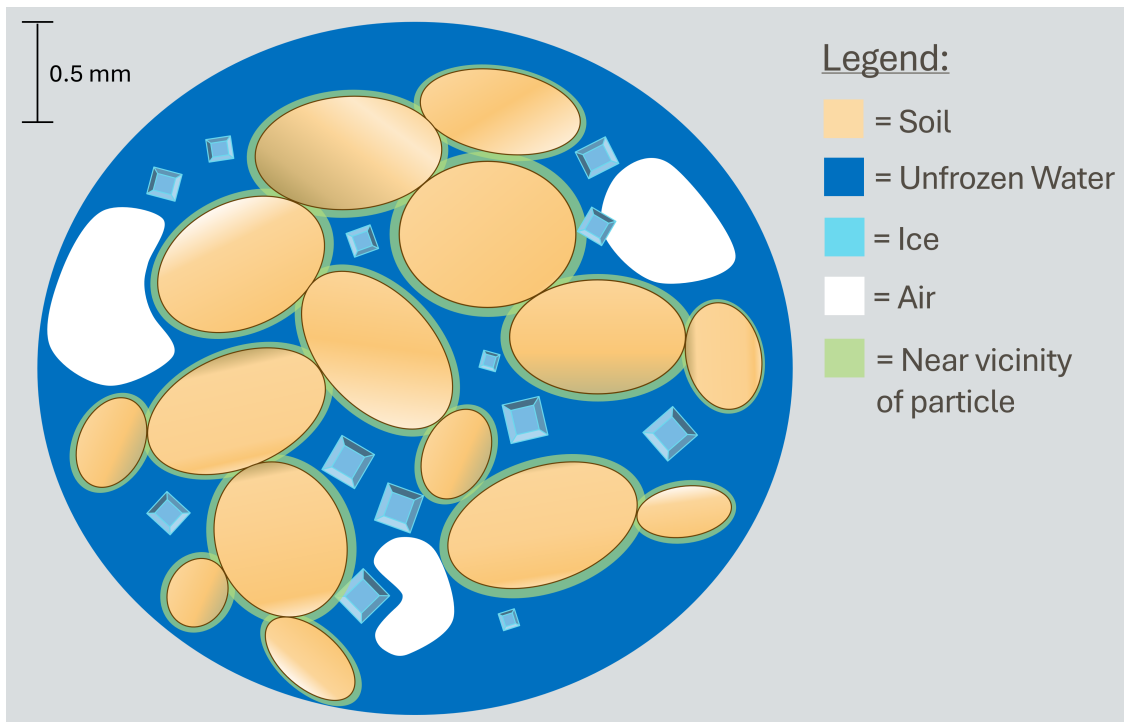


Figure 1.1: Representation of a case study soil sample as a randomly distributed multiphase heterogeneous system of soil grains, air, unfrozen, frozen and bound water.

In the relation originally presented in Sihvola, though ice was not included, the free pore water was treated as the background phase in which soil grains, air pockets and strongly

bounded water are distributed. This has been extended to include the ice phase for application in cryotic soils in the subsequent chapters (See 3.2).

1.1 Goals and Research Question

For soil freezing characteristic curves, the current conversion curve in Capacitance sensors is inadequate for i) a cryotic temperature range and ii) capturing freeze-thaw behaviour. The goals of this thesis are to:

1. Develop a new conversion curve to transform ε_{eff} into θ_{uwc} . This new conversion curve should be i) physically grounded and ii) appropriate to cryotic conditions.
2. Solve the generated conversion curve numerically. The authors of this paper have made the workflow available through MATLAB scripts that are relatively accessible to the un-initiated programmer.
3. Develop an equation that encompasses soil parameters that allow for an adaptable conversion curve tailored to each soil. Specifically soil parameters that are readily available and well documented in the literature such as porosity ϕ (v/v), bulk density ρ_b , and specific surface area A_s .

These goals address the identified research gap, providing the scientific community with a methodology appropriate for the interpretation of capacitance-based measurements of unfrozen water content in cryoptic soils.

Chapter 2

Literature Review

2.1 Cold Regions Warming

In recent years, our planet has undergone unprecedented climate changes in terms of both scale and rate (Rantanen et al., 2022; Wang et al., 2023). Anthropogenic climate warming has caused the global temperatures to rise consistently for the past 5 decades ($0.18^{\circ}\text{C}/\text{decade}$), with a notable increase in the rate of warming starting in the 1990s (Samset et al., 2023). More notably still, the Arctic has been reported to warm at nearly four times the global average, driving ever greater risks for the communities, fauna, and flora inhabiting these regions (Rantanen et al., 2022; Sae-Lim et al., 2025; Sivarajah et al., 2021). The effects of this planet wide warming have yet to be fully understood or even properly parametrized and the scientific community has barely begun assessing and reporting the often irreversible changes ecosystems have undergone under this new temperature driven disturbance (Lemieux et al., 2024).

This thesis specifically focuses on the ramifications of global warming on the thawing of permafrost. Permafrost is defined as "[...] rock or soil that remains at or below the freezing

point of [0° C] for two or more years [...]" (NRCA, 1988; USEPA, 2024). Permafrost is present in cold regions of the northern and southern hemispheres, as well as in mountainous areas (Obu, 2021). It underlies nearly 22% of the exposed land surface in the northern hemisphere and over 5 millions individuals, many of whom belong to Indigenous nations, live on discontinuous and continuous permafrost (Ramage et al., 2021). The temperature of the ground and hence the stability of permafrost is inherently connected to surface temperature. As the air temperature fluctuates, so does the temperature of the ground, further impacting the temperature in its near sub-surface (CGU, 2025). In that regard, similarly to surface temperatures, permafrost temperatures have been shown to follow an upward trend as depicted in Figure 2.1 (USEPA, 2024; Biskaborn et al., 2019).

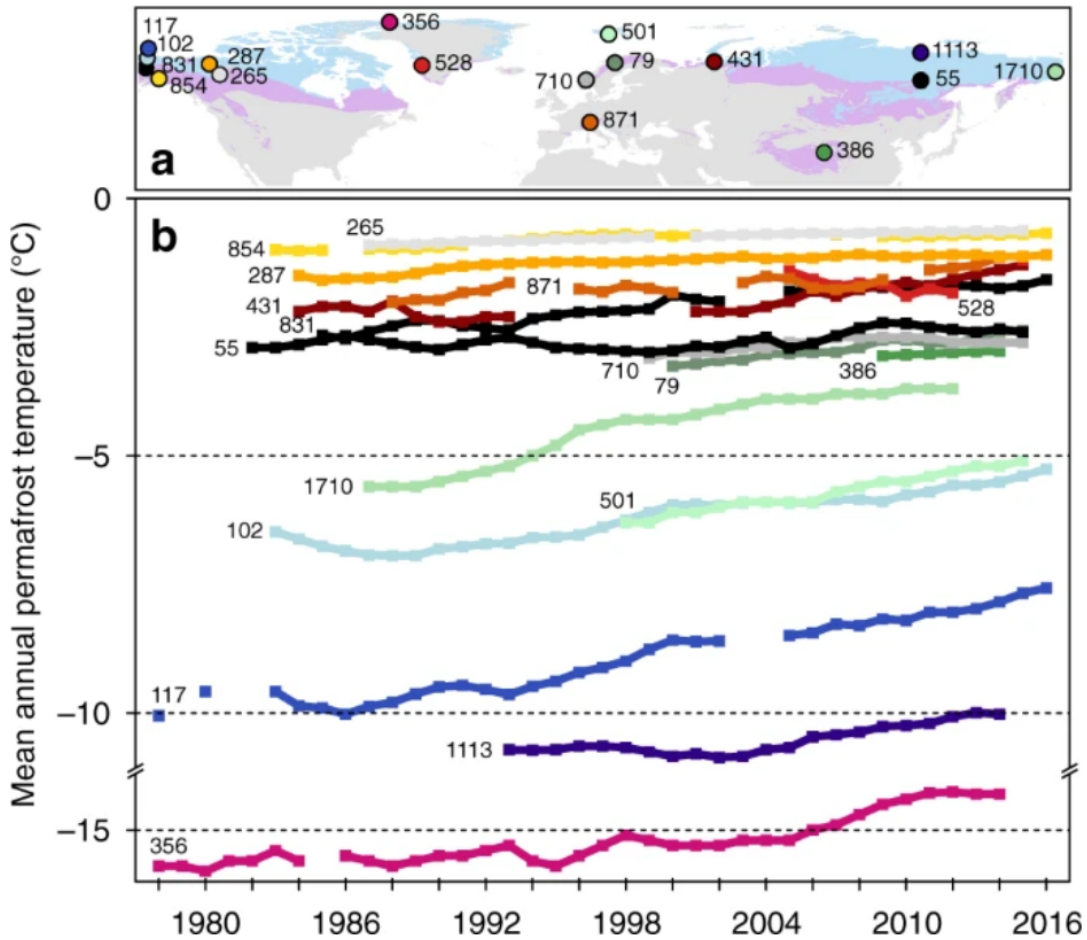


Figure 2.1: Permafrost temperature trend from 1975 to 2016 from Biskaborn et al. (2019).

The definition of permafrost, especially the part stating that it is " [...] at or below the freezing point of $[0^{\circ}\text{C}]$ for two or more years [...] " means that the soil is under cryotic conditions i.e. at a temperature T below 0°C for a substantial amount of time. However, this definition does not encompass the presence of ice in order to be deemed "permafrost" (NRCA, 1988; USEPA, 2024). The assumption is that, under cryotic conditions and given ample time, ice should form within partially or fully saturated soil. The presence of ice within permafrost is responsible for many of its thermophysical and chemical properties (Fisher et al., 2019;

Kleinberg and Griffin, 2005; Liu et al., 2018; Watanabe and Osada, 2017). Therefore, assessing how much unfrozen water content is contained in permafrost (i.e. liquid water as opposed to ice) is essential to assessing the stability and thermophysical properties of permafrost, especially as it warms (Jin et al., 2021, 2022; Walvoord and Kurylyk, 2016). Ice can only be stable in cryotic conditions i.e. $\leq 0^{\circ}\text{C}$ and, as temperature increases in permafrost, so does its unfrozen water content θ_{uwc} as the soil gradually thaws. The following section 2.2 **The Physics of Soil Freezing Processes** compiles a comprehensive overview of the theory of ice nucleation in cryotic soils, drawing a connection in between Temperature, T and unfrozen volumetric water content, θ_{uwc} .

2.2 The Physics of Soil Freezing Processes

This research requires an understanding of the fundamentals behind classical nucleation theory of ice in constrained media like saturated soils. This section describes the mechanisms that inhibit or advantage ice nucleation (subsection 2.2.2) and begins with an introduction to soil freezing characteristic curves.

2.2.1 Unfrozen Water Content: Soil Freezing Characteristic Curves (SFCCs)

Soil freezing characteristic curves (SFCCs) are physical relationships that relate volumetric unfrozen water content in soils to their temperature (Devoie et al., 2022). They display a characteristic hysteretic behavior where the freezing and thawing limbs are distinct from one another in volumetric water content θ versus temperature T. This causes the soil to have a different unfrozen volumetric water content for the same temperature T, depending on whether it is freezing or thawing.

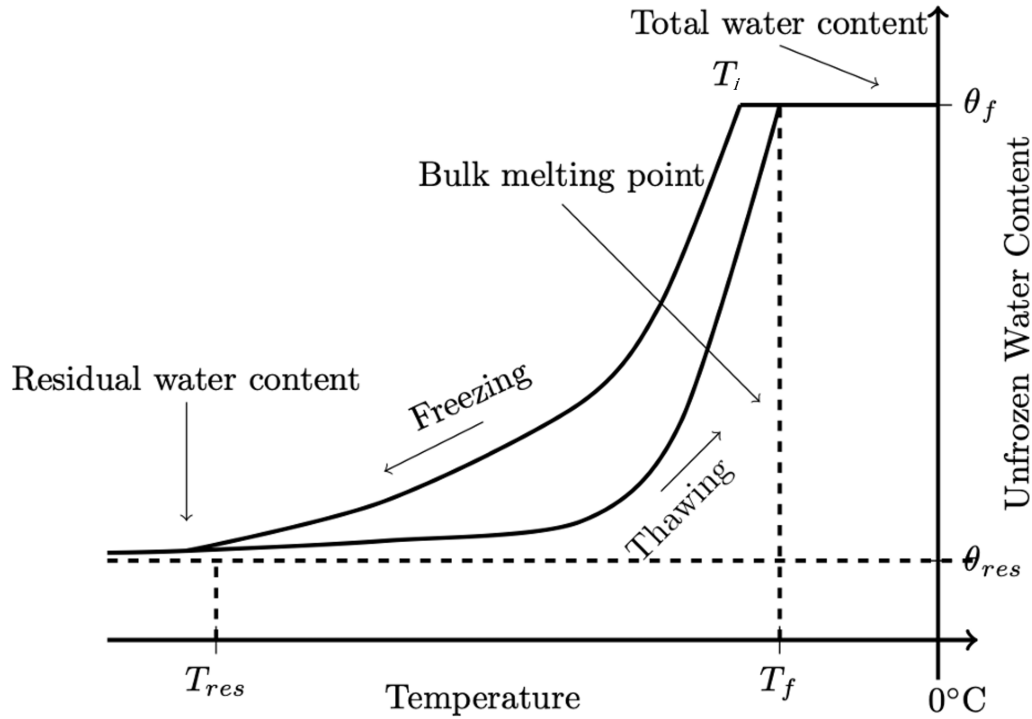


Figure 2.2: Idealized representation of a Soil Freezing Characteristic Curve modified from Devoie et al. (2022).

Sections of notable interest in any SFCC are: the initial total water content θ_f , the first trigger of ice nucleation T_i , the bulk melting point T_f and the residual unfrozen water content θ_{res} as seen in Figure 2.2. The initial total water content θ_f is the initial, fully thawed water content of the soil and has been an ongoing source of debate within the scientific community as a controlling parameter of residual water content θ_{res} (Suzuki, 2004; Williams, 1964). The first trigger of ice nucleation T_i represents the temperature associated to the first major event of ice formation of the system. The bulk melting point T_f is the temperature at which the system has fully thawed after a freezing event. The residual unfrozen water content θ_{res} or as referred to in this thesis $\theta_{unfrozen\ water\ content}$ is the amount of water that

remains in a liquid state even when the system reaches frozen stability at very low temperatures. Note that the line θ_{res} is slightly off from the "Residual Water Content" plateau. This stems from the fact that, despite often being called "unfreezable water", the amount of residual water content in soils, at low temperatures stalls and only minutely changes from $[T_{res}, -273.15^{\circ}K]$ (Joe Wolfe and Koster, 2002; Wolfe, 2025). The residual water content "plateau" asymptotically approaches the θ_{res} line: The definition of when the "plateau" starts is left to the discretion of the authors. The freezing point of water is well known to be at $0^{\circ}C$, but SFCCs frequently display T_i that are substantially below this point and elevated amounts of θ_{uwc} even at very low temperatures. These two phenomenon, namely the depression of the freezing point of water and the residual unfrozen water content, are two unusual properties of water which show up in SFCCs and hold considerable value for cold region scientists.

2.2.2 Nucleation of Ice

Ice nucleates at temperature, T_i , a temperature defined by the complex thermodynamics of ice crystallization. One of the definitions of a crystalline phase is: "A solid is a crystal if its atoms, ions and/or molecules form, on average, a long-range ordered arrangement [...]" (Grimm, 2015). This order at the atomic range constitutes 3-dimensional "patterns" which are referred to as crystal lattices. These crystalline structures are fundamental in understanding both crystal nucleation processes and crystal physical properties. Ice is a fairly "simple" crystal because it is the solid phase of pure water (H_2O), without any inclusions or ionic content. For the pressure conditions discussed in this thesis (and for most of those naturally present on planet Earth), the only naturally occurring morphological forms of ice belong to the hexagonal crystal family (Chaplin, 2021). For systems under higher pressure

or non-cryotic conditions, the water ice formed belongs to different crystal families, discussed in other work such as Hermann et al. (2012), and are beyond the scope of this study.

The nucleation of crystalline phases requires the molecules/atoms to move and reorganize themselves in order to crystallize. Anything that may inhibit the realignment of the constituents of the crystal lattice actively hinder the formation of the crystal. In thermodynamics, we often discuss *nucleation rate* and *nucleation work*. Nucleation rate is the frequency at which the system attempts to "create/transition" into the new phase (ice) and nucleation work is the amount of work [J] needed to overcome the activation energy required to have a stable new phase in equilibrium with its surroundings (Maeda, 2021). Fundamentally, when a substance (water) transforms into a new phase (ice), there will be a place in the system where the two phases are in contact. This will cause an interfacial boundary between the thermodynamically stable phase (ice) and the metastable parent phase (water). This interfacial boundary costs a certain amount of free energy from the bulk (system) to be created and maintained, depending on its total surface area. For a specific pressure-temperature at which the phase change is occurring, the activation energy requirement for an ice crystal of radius r to exist and persists varies. Classical Nucleation Theory (CNT) tells us that the activation energy is defined as $\Delta G(r)_{activation} = \Delta G(r)_{bulk} + \Delta G(r)_{interfacial}$ where ΔG represents the change in free energy for the bulk (system) and the interfacial boundary between the phases (See Figure 2.3).

For a mildly supercooled system ($T < 0^{\circ}\text{C}$, cryotic conditions), the formation of the first ice crystal will generate the need for an interfacial energy boundary between the two phases

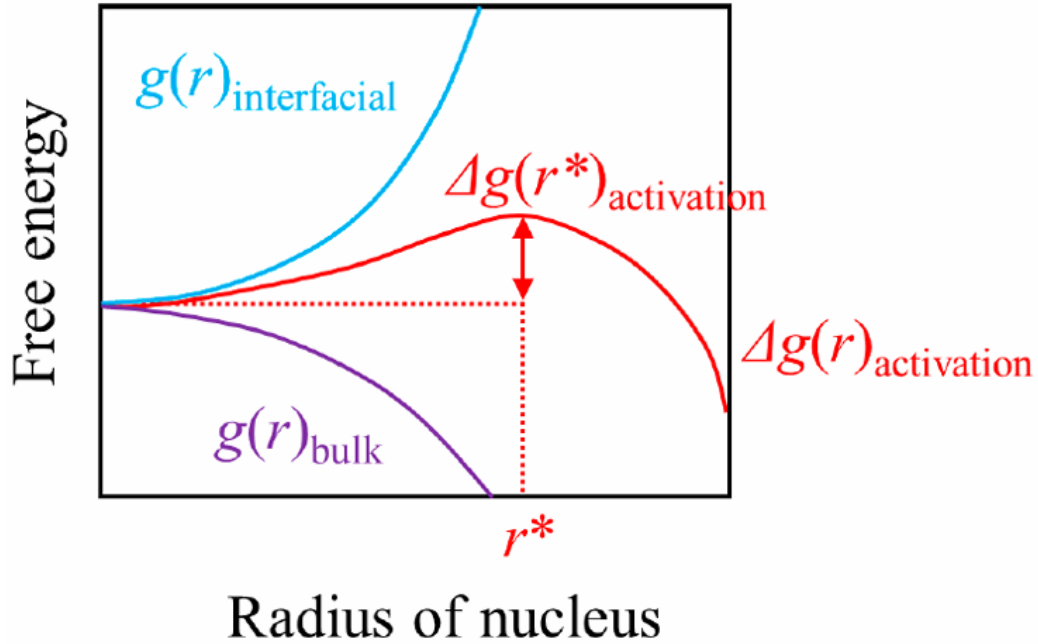


Figure 2.3: The activation energy barrier and its relationship to the radius r of a crystal nucleating in a medium from Maeda (2021).

present in the system. As the bulk system loses free energy to generate the crystal, the interface energy will grow. Because the $\Delta G(r)_{bulk}$ is proportional to the cube of r and the $\Delta G(r)_{interfacial}$ is proportional to the square of r there will exist a radius r^* for which the $\Delta G(r)_{activation}$ will decrease with an increasing r i.e. $\frac{\partial \Delta G(r)_{bulk}}{\partial r}$ becomes negative. This is what is commonly referred to as the "critical nucleus size" for which a crystal of nucleus $\geq r^*$ will both be stable and able to grow, leading to the continued transformation of water into ice. Nuclei that are $< r^*$ will be unstable and melt back into the liquid phase. This principle is known as the "Gibbs Free Energy", or the tendency of a process to proceed spontaneously in the direction of negative Δ free energy (Atkins and De Paula, 2006).

For an extremely cold system, the $\Delta G(r)_{bulk}$ would fall rapidly because the "driving force"

or nucleation rate of ice crystals is much greater. The colder the system, the more unstable the liquid phase and the more prevalent the ice phase, but the decrease in temperature also limits the kinematic energy of the molecules. This competing factor prevents or slows the rearrangement of the molecules into crystalline lattices. This phenomenon known as "petrification" is prevalent in substances that are cooled very rapidly or supercooled, where the viscous slowdown effect associated with low temperatures results in incomplete crystallization. In these systems, despite having a near absent activation barrier energy, a heavily supercooled system nucleates ice crystals poorly because of the low thermal energy limiting the kinetic factors (i.e. mobility) of the molecules.

This kinematic factor is not only affected by temperature, but also by other forces at play within soil systems. For example, strongly bound water (water with a dipole interaction with the soil matrix) will also be harder to freeze than free water because of how "viscous" it is. Strongly bound water is said to have lower potential energy and will require more activation energy to orient its water molecules into crystalline lattices than free bulk water (Joe Wolfe and Koster, 2002). This relationship is based on the distance from the surface binding the water, where the "first shell of hydration" will be more strongly bound than a further layer. The surface binding the water in itself can also affect the degree of hydration, how hydrophilic it is and how strongly it induces a dipole in the nearest water molecules will affect the strength of the dipole-dipole bond and further decrease the kinematic factor. This in turn affects the nucleation rate of ice crystals in those water layers. This theory closely resembles the Stern-Gouy electrical double-layer theory which stipulates that intermolecular forces between bound water molecules and nearby surfaces create a bound water structure composed of a strongly bound layer (adsorption-layer) and weakly bound layer

(diffuse-layer) (Allagui et al., 2021; Dobson et al., 1985; Liu et al., 2020). This "strongly and weakly bound water" is often grouped under the umbrella term of "hygroscopic water" and considered to be the last water to possibly freeze because of its low kinematic factor.

Another better known phenomenon which causes ice to nucleate below 0°C is the impact of solutes on the freezing point depression of solutions (Atkins and De Paula, 2006). Pure water is expected to have a freezing point of 0°C, but the actual phase change of liquid water to ice frequently occurs under supercooled conditions i.e. $T < 0^\circ\text{C}$. In that same vein, the addition of solutes in water can greatly depress the expected freezing point of water below 0°C. This phenomenon is once again related to the crystalline structure of ice: because ice is an orderly crystalline substance at the atomic scale, the more "random" the liquid trying to crystallize is, the harder it will be for it to crystallize. The measurement of "randomness" of a solution is referred to as its entropy and it increases the more solute in solution it has. This key concept of thermodynamics is the reason we salt the road in winter to melt the ice, or add salt to pasta water to depress the boiling point (and for taste). In all of these examples, solutes in solution are excluded from the solid crystalline, partitioning into the liquid phase of a system rather than the solid (or gas) phase of a two-phase system. This fundamental concepts of component partitioning underlies magma cooling sequences and is often dependent on the phase change rate (McCarthy et al., 2023). These concepts also apply to simpler water solutions undergoing freezing: in essence, the cooling of magma and the formation of mineral phases is a more complex expression of a water solution crystallizing a simpler mineral phase, namely ice.

2.3 Estimate of θ_{uwc} : SWCC to SFCC

The wetting and drying cycle of soils is frequently used as an analog to obtain the freezing and thawing cycle of soils (Kurylyk and Watanabe, 2013). In both cases, the phenomena are hysteretic: in θ_{uwc} vs temperature (T) space for SFCCs and in θ_w vs pressure (P) space for SWCCs. Despite both displaying hysteresis, the underlying mechanisms which causes hysteretic behavior differs. In freeze-thaw, the freezing and thawing limbs are distinct because of the natural tendency of water to easily supercool. Because ice is a crystalline phase, the first ice nucleation governs the temperature at which phase change will actually occur. Due to the difficulty related to the formation of this first ice crystal, water very easily supercools below the expected bulk freezing point, causing it to diverge from its thawing limb which is not subject to the same nucleation process. The phase change of water to ice is far more thermodynamically complex to predict than the one from ice to water because of the crystalline nature of ice: molecules need to reorient themselves into crystal lattices and the interfacial and bulk energy of the system need to balance one another out to achieve a stable ice crystal. As for wetting and drying, hysteresis occurs because of the difference in entry and exit pressure for water in pores (Mady and Shein, 2020). Usually, soil moisture for the drying curve is larger than its value for the wetting curve, inferring that water more easily enters pores than it leaves them. This is because of the aptly named "ink bottle effect", depending on the current state and history of the system, different sizes of pores control the water retention of the soil. During drying, the water content in the soil is controlled by the narrow points between pores whereas during wetting, water retention is controlled by the widest points in the pore cavity. Similarly to SFCCs, the pore networks connectivity, size and distribution also govern the hysteresis behavior where larger pores more easily drain than smaller ones and dead-end or poorly connected pores trap water in SWCCs (Cihan et al., 2014).

Despite their physical differences, predictive SFCCs models are frequently based on their SWCC equivalent because of a common factor that both govern their hysteresis: entrapment of water in pore space due to both sorptive (bound water) and capillary forces (Kurylyk and Watanabe, 2013). In both freezing and desiccation limbs, the desaturation process (removal of liquid water) is governed and hindered by sorptive and capillary forces. This parallel was first explored and explained by Koopmans and Miller (1966) who showed that the analogy was correct for both sorptive (SS soil i.e. solid–solid contact between particles) and capillary (SLS soils i.e. solid–liquid-solid contact) dominated soils (Koopmans and Miller, 1966). Usually, SS soils are sand or silt rich and SLS soils are clay rich. This is mostly due to the shape, arrangement and pore structure of the components of the soil: the plate-shaped clays tend to align in sheet-like structures while the more granular sand and silt organizes in rigid, capillary-like pores (Bhavya and Nagaraj, 2025; Kuehn et al., 2024). The varying grain size, shape, geometrical arrangement and pore network connectivity causes either sorptive or capillary forces to control the behavior of the water in the pores, affecting the distribution and nucleation of ice crystals during freezing and to an extent the distribution of unfrozen water in both the freezing and thawing limb.

Based on the capillary and sorptive forces, the formulation of predictive SFCC relationships has been heavily influenced by capillary theory i.e. the behavior of liquids in narrow spaces due to pressure gradients and the interplay of cohesive and adhesive forces (Kurylyk and Watanabe, 2013). Following capillary theory, an SFCC derived model by Koopmans and Miller (1966) equated the specific energy of air-water and ice-water interface for SWCCs and SFCCs respectfully. The pore water gauge pressure for drying in ice-free soil can be

related to the pore water gauge pressure for freezing in air-free soil, assuming that the ice and air pressure is equal to atmospheric pressure. They also concluded that their model was only applicable to soils which are dominantly either SS or SLS and that the drying curve can only be an analog to the freezing curve while the wetting curve only an analog to the thawing curve. Despite being restricted to only 2 phase systems, the model from Koopmans and Miller (1966) started a long line of SFCC models from SWCC characteristics. In their derivation, the use of the Clapeyron Equation to relate SWCCs to SFCCs has been common practice in recent scientific literature Li et al. (2023); Wang et al. (2024). The benefit of the Clapeyron equation comes from its ability to translate the primary independent variable of SWCCs, pressure, into the primary independent variable of SFCCs, temperature.

SFCCs Predictive Relationship not from SWCCs

The development of SFCCs has also been done independently of SWCCs (Anderson and Tice, 1972; Anderson and Morgenstern, 1974; Wu, 1977; Kozlowski, 2007; McKenzie et al., 2007). Any mathematical model/simulation aiming to represent the freezing and thawing of soil system needs to encompass a representation of the SFCC and many researchers have chosen to derive their SFCC relationships through simplified mathematical approximations. For example, Anderson and Tice and Anderson and Morgenstern found that the relationship between the liquid water content and the temperature of freezing soils could be approximated with a power law relationship given that the unfrozen water content is presumed to be independent of total water content. Another frequently applied mathematical representation used for SFCCs models are piece wise linear functions which help capture the hysteretic behavior of freezing and thawing cycles in soil (Wu, 1977; McKenzie et al., 2007). Continuous exponential functions have also been used for SFCC models McKenzie et al. (2007); Ge et al. (2011).

2.4 Hysteresis

The definition of hysteresis that is applicable and relevant to soil science is the following: " [...] the dependence of the state of a system on its history"(Bertotti and Mayergoyz, 2014). Despite its simplicity, this definition holds a lot of complexity. As seen in Figure 2.2, an idealized SFCC is perfectly hysteretic: it has a distinct freezing and thawing limb. Looking back at the definition of hysteresis, the "dependence of [the system] on its history" here implies that the unfrozen water content θ_{uwc} of our system is dependent not only on the temperature T, but also on the previous states the system was in. This essentially "vectorizes" our data: depending on the "direction the system" is going i.e. undergoing freezing (negative $\frac{\partial T}{\partial \text{time}}$) or thawing (positive $\frac{\partial T}{\partial \text{time}}$), the θ_{uwc} value for a given change in temperature differs. This simple yet highly complex concept now requires knowledge of both the past (previous value), but also the present (current value) of the system to understand its future (next value). SFCCs represent Θ_{res} (unfrozen volumetric water content) vs T (Temperature) and only intrinsically have a time dependency (t) (See Figure 2.4). This come from the experimental procedure used for Freeze-Thaw experiments which utilize Temperature Time Programs to precisely modulate the temperature of saturated soil samples (See Appendix A).

Much of the existing SFCC studies are lab-based, however natural systems i) rarely equilibrate before undergoing further temperature change and ii) are rarely monotonic i.e. the temperature fluctuates up and down constantly. A system will often be composed of one "major hysteric loop" and several smaller "sub-loops" or "scanning curves". The major hysteric loop describes the limits of the path the system undergoes when an entire cycle is completed. However, the temperature evolution $\frac{dT}{dt}$ which dictates the direction the system

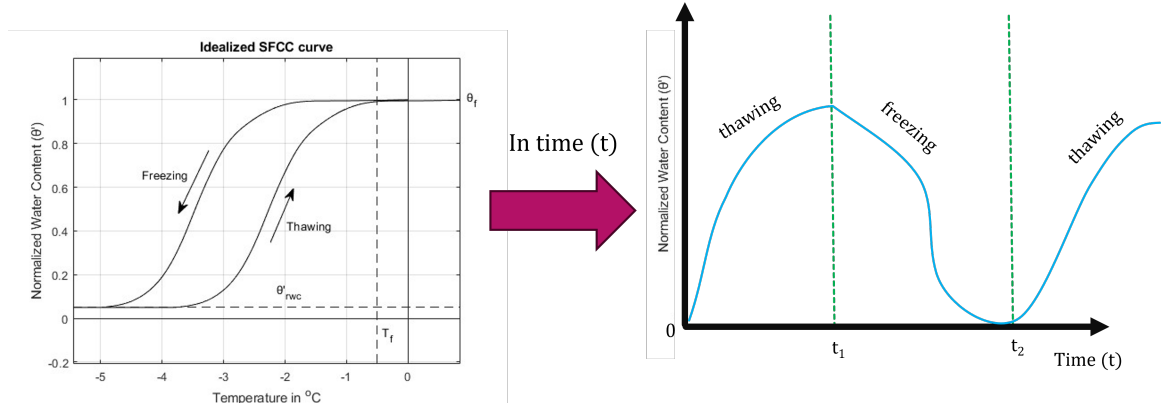


Figure 2.4: Depiction of the connection between SFCCs (left) and hysteresis (right). The SFCC on the left side does not encompass any temporal dependence, despite its "raw data" being time dependent. The hysteresis is apparent once the time dependence t is shown/kept (right). Time t_1 and t_2 are "reversal points" where the freeze-thaw direction of the temperature evolution in the system is reversed.

is undergoing given time t may not i) equilibrate or ii) strictly decrease (or increase) until completion of the current freezing or thawing limb. This causes the system's direction to change mid-cycle and produces a new path in θ_{uw} vs T space called a scanning curve. These secondary freezing/thawing curves are restricted to the domain bounded by the major hysteretic loop, but are also subject to their own hysteric behavior 2.5.

As mentioned previously, hysteresis is both present in freezing-thawing and in wetting-drying cycles of soils. However, the mathematical description of hysteresis has only been used for predictive models of wetting-drying data (Bertotti and Mayergoyz, 2014; Mualem, 1973; Wei and Dewoolkar, 2006). Application of a generalized Preisach model to soil-moisture hysteresis have been suggested as a predictive relationships of SWCCs (Mayergoyz and Friedman, 1988; Sarker et al., 2020). No mathematical model of hysteresis in SFCC predictions exists to date.

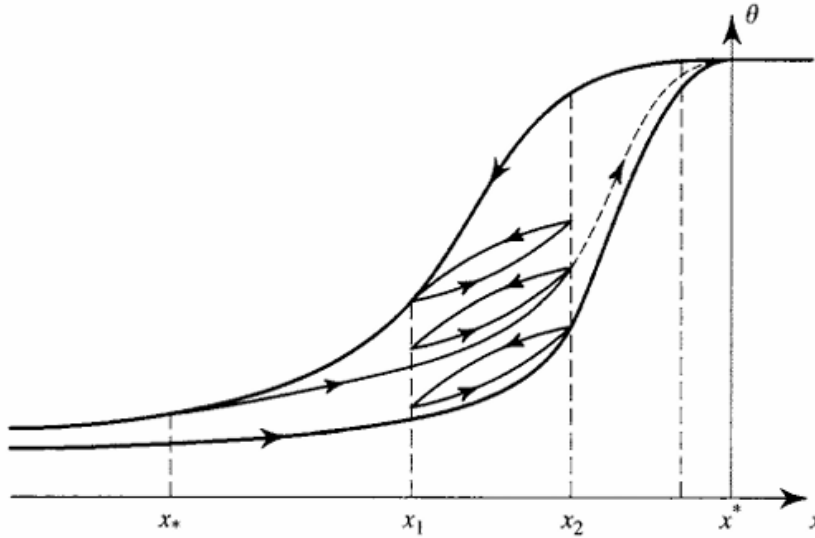


Figure 2.5: Theoretical scanning Curves for a hysteretic system from Bertotti and Mayergoyz (2014). Notice the dotted scanning curve which approaches the main hysteretic curve asymptotically before reconnecting to the main hysteretic loop at x^* .

2.5 Measurement of θ_{uwc} : Instrumentation

The fundamental challenge of measuring unfrozen water content in cryotic soils is assessing the ice content in a non-destructive and replicable manner. Several techniques have been developed, each with their own merits and shortcomings when it comes to field and laboratory settings, especially regarding precision and accuracy. Early methods for the quantification of unfrozen water content were based on the thermophysical properties of ice. One of the first recorded attempts of θ_{uwc} measurements is from *Bouyoucos, 1921* who used the difference in volume between water and ice to infer the ice content of samples in cryotic conditions, termed dilatometry (Boutoucos, 1921). From there, the scientific community experimented with calorimetry, using the difference in specific heat capacity (C_{water} and C_{ice}) (Anderson and Tice, 1972). Advancements in microelectronics allowed the community to leverage electrical properties such as capacitance and impedance leading to measurement

techniques based on capacitance sensors and time domain reflectometry (Dyck et al., 2019; He et al., 2016). Because of their practicality and low cost, capacitance and Time Domain Reflectometry (TDR) methods remain the preferred instrumentation for field and some laboratory measurements for many researchers. In modern lab settings, spectroscopy based measurement techniques like Nuclear Magnetic Resonance (NMR) have brought improved accuracy for laboratory tests (Tian et al., 2014; Zou et al., 2023).

2.5.1 Field Measurement Techniques

Fundamentals: Capacitance

The current most widely used instruments for the measurement of unfrozen water content in cryotic soils are capacitance-based sensors. Capacitance measurements estimate water content of soils based on their dielectric permittivity. Dielectric permittivity is the property of a material to hold an electrical charge, exactly like a capacitor would in a circuit board. Capacitance sensors work exactly on that basis: once properly installed within the soil, the two probes of the sensor measure the time required for the medium between them to reach a certain charge indicative of the soil's apparent dielectric permittivity (METER, 2025b). Because the dielectric permittivity of ice ϵ_{ice} is ~ 3.00 and the dielectric permittivity of pure water is ~ 80.00 , the more ice in the soil, the lower its dielectric permittivity (Evans, 1965; Malmberg and Maryott, 1956). This elegant yet simple correlation is what underlies the principle of the apparent permittivity, $\epsilon_{apparent}$, as a proxy measurement for θ_{uwc} . Dielectric permittivity is a complex (*i*) measurement with both a Real part, \mathbb{R} , which is correlated to polarization factors and an imaginary $Im(\mathbb{Z})$ component which is related to the dielectric losses, both of which are frequency dependent measurements (Ellingson, 2020). For the application of the capacitance sensor, only the $\mathbb{R}|\epsilon_{apparent}$ is relevant. Note that the frequency

for the electrical current in the capacitance sensor is chosen based on the range of maximum sensitivity of $\mathbb{R}|\epsilon_{apparent}|$ to dipolar processes (Mauritz, 2014).

Fundamentals: TDR

Time Domain Reflectometry (TDR) is an interferometry measurement technique that uses frequency dependent dielectric permittivity measurement to infer θ_{uw} (Smith and Tice, 1988). Similarly to the capacitance method, TDR uses the apparent dielectric permittivity of a sample as a proxy for residual unfrozen water content. TDR works similarly to a radar: An electrical signal is sent down a conductor (electrical cable) and the sensor "listens" for any reflection. Upon reaching regions of stark contrasting impedance, the signal will partially reflect back to the emitter while also pursuing its course towards the receiver. Based on the interference patterns received, it is possible to reconstruct the impedance of the medium. There are currently two applications of the TDR method in instrumentation: i) a time measurement is taken, similarly to the Capacitance method, for a conductor of known distance L and converted to dielectric permittivity with a simple propagation relationship or ii) a complete set of both the signal recorded by the emitter and receiver is spectrally analyzed, and magnitude and interference pattern (delays and phase shifts) are assessed to characterize the medium (Jones, 2002). Case i) follows the same principles as the Capacitance method, beyond the underlying principle on which $\epsilon_{apparent}$ is obtained. For the Capacitance method, the medium is treated as a simple capacitor and for case i) of the TDR method, the medium is treated as a simple impedance medium.

Though both TDR and Capacitance-based sensors both measure dielectric permittivity, $\epsilon_{apparent}$ is measured and interpreted differently in TDR, where interferometry is used to

infer permitivity from wave propagation and interference patterns. A similar dielectric mixing model is needed to convert $\epsilon_{apparent}$ to θ_{uwc} but uses both $\Re|\epsilon_{apparent}$ and $Im(\mathbb{Z}|\epsilon_{apparent})$ depending on the input frequency f . Recent work like Dyck *et al.*, 2019 demonstrate the complexity of mixing models when physical processes like strongly bound water and dual porosity are tackled in the conversion model (Dyck *et al.*, 2019).

One of the issue with TDR is the complications related to continuous long lasting field measurements. In cold regions, soil will heave and subside as it undergoes freeze-thaw cycles annually, bending or even breaking the sensitive coaxial cable, which is also sensitive to environmental factors such as wildlife. Significant maintenance and monitoring is required to ensure that the apparatus is both functional and accurately collecting data, resulting in, many short-lived field TDR setups.

2.5.2 Lab Measurement Techniques

Fundamentals: NMR

Nuclear Magnetic Resonance is a spectroscopy measurement method which has gained traction in the scientific community for its high accuracy and precision to represent θ_{uwc} (Smith and Tice, 1988). Atomic nuclei have magnetic moments that are characteristic for each substance and stable phase. When put under an electromagnetic field, atoms will adsorb a portion of the radiated energy and realign themselves within the electromagnetic field. If adjusted to match the frequency associated to the hydrogen proton associated with liquid water (10.72 MHz), NMR can be used to detect liquid water within mediums because a drop in signal intensity will indicate the formation of ice in a freezing medium. By applying a

pulse of radio frequency to magnetized protons, a temporary disturbance can be caused in their alignment. The energy emitted by the realignment or spin of the protons is read as a voltage which decays as the realignment ends. The voltage decay curve read by the NMR apparatus is also called a free-induction decay (FID) curve and is the raw data reported in NMR. The other information of interest is the spectra of the FID called the T_2 relaxations times which is a Fourier transform of the FID. Since the peak value of the FID is directly proportional to the number of protons in a medium, if the NMR apparatus is set to detect H_2O , a peak in the FID signal would indicate the presence of water in a medium. The final Fourier Transform spectrum (T_2) can then be analyzed for peaks and troughs in signal magnitude at particular frequencies to characterize the water content of the analyzed sample as liquid or ice, and can even be used to distinguish the forms of ice (Callaghan et al., 1999; Cameron et al., 1985; Lei et al., 2022).

There are several challenges in NMR measurements: i) the calibration of the apparatus, ii) the cost of the system, iii) the limited sample size and preparation. Like most spectroscopy measurement methods, NMR requires extensive calibration procedures to assess the relevant range of frequencies (Ktigel-Knabner, 1997). Depending on the material of interest, study of its molecular properties is required to determine the characteristic spectra needed to determine the presence, quantity, and distribution of the phase of interest. NMR systems are expensive and highly regulated due to their use of nuclear material. Access to NMR systems can be challenging, especially for solid-state NMR. The final challenge of NMR measurements is the design of the sample holder. Most NMR sample tubes are small and narrow which causes a lot of edge effects between the sample and the tube. These constrained boundary conditions differ from the ones found for soils in field or lab settings and

induce errors in the measured freezing behavior that haven't yet been constrained. Development of larger temperature-controlled NMR ready holders for larger samples is technically challenging due to the measurement technique but would pose a great advancement to the field. In the case of NMR, the raw data conversion is more of an analysis of characteristic spectral signal based on molecular properties and less of a conversion curve, but the challenges of accurately converting the raw measurements of the apparatus into θ_{uwc} remains the same.

2.6 Conversion Curves: From measurement to Ice content

Something which all of the previously mentioned measurement techniques have in common is that they do not directly measure the unfrozen water content of soils, but rather convert a proxy measurement into water content based on a certain conversion curve/analysis. For capacitance, this proxy value would be the ϵ_{sample} or ϵ_{eff} . All measurement techniques report a voltage, resistance, volume change, spectral signal, or other raw data which requires conversion to volumetric unfrozen water content. This conversion has potential to introduce significant error to the system. Great importance should be given to the accuracy, precision, reliability and applicability of the conversion curve applied to the raw data depending on the instrument, nature of the sample and presence of water, air and/or ice in the sample.

Through this lens, a thorough literature review and assessment of current techniques and standards for electromagnetic based sensors was conducted to assess areas where improvement could be made. Simply put: Sensors are only as good as the conversion curves used to report the data you're truly interested in. The best sensor precision and accuracy becomes close to meaningless if the data reported is poorly converted.

2.6.1 The Current Conversion Curve: The Problem with *Topp, 1980*

The current conversion curve used in most readily available soil moisture sensor is the *Topp, 1980* equation (Topp et al., 1980) (See Eq. 2.1). This equation is a third degree polynomial empirical fit from an agglomeration of SWCC data of largely different soil types. In its design, it was never envisioned to be used in cryotic conditions ($<0^{\circ}\text{C}$) yet it is one of, if not the most, widely used conversion curves used for SFCC data acquisition. This limits our capacity to measure unfrozen water content in soils because i) the conversion was never intended to be used in the $<0^{\circ}\text{C}$ temperature range and was never validated for this range, ii) empirical fits made on large datasets of various soil types yield an uniformizing behavior, iii) the *Topp, 1980* equation in itself does not encompass parameters of physical significance (See Equation 2.1) and iv) the conversion lacks any level of representation or connection to phase change of water to ice.

$$\theta_{\text{water}} = 4.3 * 10^{-6} \varepsilon^3 - 5.5 * 10^{-4} \varepsilon^2 + 2.92 * 10^{-2} \varepsilon - 5.3 * 10^{-2} \quad (2.1)$$

Due to its empirically fitted nature, the *Topp, 1980* equation is not transferable from one soil type to another without yet another empirical fit. This is because it doesn't allow physically meaningful parameters from samples metadata to be used to characterize soil types. As further expanded in Section 3, soil types greatly influence dielectric readings and specific attention should be given to their proper parametrization.

2.6.2 Dielectric Mixing Models

Dielectric mixing models are mathematical relationships that express the apparent dielectric permittivity of heterogeneous substances based on the dielectric permittivity of their constituents. A perfectly accurate mixing model is impossible to achieve, but they often approximate real world samples so accurately that the mixing prediction can be used to characterize materials. Work like Sihvola demonstrates the use of dielectric mixing models for characterizing heterogeneous geophysical or subsurface materials (Sihvola, 2000). A clear example of the derivation of a mixing model is presented in Sihvola's dielectric models from his 2000 paper "Mixing Rules with Complex Dielectric Coefficients". This model is developed for a soil-water-air system, considering the interactions between these three phases. Soils are highly complex and heterogeneous material which cannot be perfectly described by mathematical relationships. A stochastic average is thus needed to obtain a statistically representative and relevant average for the entire substance. According to Sihvola, the permittivity of this three-phase system can be represented by Equation 2.2:

$$\epsilon_{eff} = \epsilon_e + 3\epsilon_e \frac{\sum_{n=1}^N \theta_n \frac{\epsilon_n - \epsilon_e}{\epsilon_n + 2\epsilon_e}}{1 - \sum_{n=1}^N \theta_n \frac{\epsilon_n - \epsilon_e}{\epsilon_n + 2\epsilon_e}} \quad (2.2)$$

where θ_n is the volume fraction of the inclusions of the n th phase in the environment e and ϵ_n is the dielectric permittivity of the inclusion. In this formulation, it is assumed that: the inclusions (any other phase than the background "environment" phase) are isotropic and their shapes are spherically symmetric (Sihvola, 2000). This helps simplify the dielectric mixing model by allowing the 3-dimensional depolarization parameters to be 3-dimensionally identical, allowing the inclusions to be randomly oriented in space with no impact on their dielectric contribution to ϵ_{eff} .

Temperature dependence of dielectric permittivity of water phase

The dielectric permittivity of substances are quite dependent on temperature (Baker-Fales et al., 2023; Rayssi et al., 2018). The dielectric permittivity of pure water at room temperature is often approximated as ~ 87.0 , but actually has a noticeable negatively correlated temperature dependency for $T \geq 0^\circ C$. From the work of Malmberg and Maryott, water in positive temperature T space i.e. $T > 0^\circ C$ has a dielectric permittivity with the following dependency:

$$\epsilon = 87.740 - 0.40008 * T + 9.398 * 10^{-4}T^2 - 1.410 * 10^{-6}T^3 \quad (2.3)$$

where ϵ is its dielectric permittivity and T its temperature in $^\circ C$ (Malmberg and Maryott, 1956).

Bound water Content and Dielectric Permittivity

$V_{\text{bound water}}$ represents the volume of strongly bound water in a soil, correlated to the adsorption force, specific surface area, and electric dipole potential of the soil grains. The Stern-Gouy electrical double-layer theory informs the basic plate model used here (Dobson et al., 1985):

$$\theta_{\text{sbw}} = \delta * A_S * \rho_b * 10^{-4} \quad (2.4)$$

where θ_{sbw} is the volume fraction (v/v) of strongly bounded water content, δ is the thickness of the layer of strongly bounded water [\AA], A_s is the specific surface area [m^2/g] and ρ_b is the soil bulk density [g/cm^3]. The δ parameter is kept consistent as 5 \AA , the average representative thickness of strongly bounded water for all studied soils (Jin et al., 2020; Shang et al., 1994; Olphen, 1964; Verwey, 1947). The dielectric permittivity of water changes depending on the degree of dipole interaction with the soil matrix i.e. how strongly bounded to a surface the water is. The dielectric permittivity of strongly bounded water is approximated to equal 9.0 based on the work of Jin et al..

2.6.3 Other Models

Several empirical fits like the *Topp, 1980* equation or Dielectric Mixing Models including the Power Law or the de Loor model have been developed and used to described the dielectric permittivity of soils (He et al., 2016). Though the *Topp, 1980* equation fails to capture much of the complexity related to the phase change of water in physical systems, other existing models like the Power Law or de Loor model each present similar challenges. The Power Law model like the *Topp, 1980* model fails to capture phase change, crystal nucleation or heterogeneous soil with physically meaningful parameters (Birchak et al., 1974; Dobson et al., 1985). The Power Law model, presented in equation 2.5 is an empirical fit with a "mixing model constant" α which doesn't have a physical basis, n is the number of phases in the system, :

$$\epsilon_{eff}^\alpha = \sum_{j=0}^n \phi_j \epsilon_j^\alpha \quad (2.5)$$

This limits the transferability of the Power Law model from one soil to another.

As explained by Sihvola and Kong, the de Loor model has an issue regarding the domain over which it is valid (Sihvola and Kong, 1988). De Loor includes a ϵ^* term in the model that represents "[...] the immediate surroundings [of] an effective 'internal' dielectric constant ϵ^* [...] quantify[ing] all interactions and spatial irregularities of the other granules[...]" (de Loor, 1968). Sihvola correctly pointed out that, for a single phase material, the $\epsilon_{eff} \neq \epsilon_{inclusions}$ unless the assumption that $\epsilon^* = \epsilon_{eff}$ is made, in which case it reduces to the Polder-van Santen formula (Polder and van Santeen, 1946). This case of ϵ^* is of particular interest since the "near vicinity" of particles is the strongly bounded water adsorbed onto soil or organic matter. The assumption that $\epsilon^* = \epsilon_{eff}$ is categorically incompatible with the formulation of a mixing model in natural soils where the dielectric permittivity of strongly bound water varies greatly from both free water and the ϵ_{eff} .

The aim of this thesis is to modify the dielectric mixing models present in literature to accurately represent a multiphase heterogeneous soil system composed of soil particles, liquid water, and ice. This model will use the characterization of the bulk dielectric permittivity of the system as a proxy for unfrozen water content, and have soil-specific parameters allowing it to be transferrable to various soils.

Chapter 3

How to Assess Unfrozen Water Content Using Capacitance Sensors in Frozen Soils: A New Physics Based Conversion Curve

Quentin “Quinn” Sapin^a (she/her) [q.sapin@queensu.ca] and Élise Devoie^a (she\they) [elise.devoie@queensu.ca]

^aQueen’s University, Civil Engineering Department, 58 University Ave, Kingston, ON K7L 3N9, Canada.

Abstract

Climate warming is driving the rapid thaw of permafrost and loss of ground ice in seasonally freezing soils, but our current ability to measure these changes is actively hampered by the challenges of measuring unfrozen water content of cryotic soils. One of the most widely used techniques to measure the unfrozen water content of cryotic soils is to monitor their apparent dielectric permittivity. Paired with an empirical calibration equation or a dielectric mixing model, this measurement of dielectric permittivity, ϵ_{eff} , gives an estimate of

unfrozen water content in soils. The conversion curve selected is crucial to the quality and accuracy of the reported unfrozen water content, θ_{uwc} , a failure to appropriately transform ϵ_{eff} into θ_{uwc} can lead to significant error. This paper presents a new multiphase dielectric mixing model as a conversion curve from ϵ_{eff} to θ_{uwc} based on soil-specific parameters. The derivation of the conversion curve and its performance on laboratory experiments of fully saturated soil samples are presented. The application of the new multiphase dielectric mixing model rather than the traditional, widely used third-degree polynomial from Topp et al. considerably alters the final θ_{uwc} reported: the residual water content is almost three times that reported by Topp et al., 1980. Such considerable error margins in residual unfrozen water content dramatically alters a soil's hydrothermal-mechanical properties such as strength, thermal conductivity and permeability which can lead to different behavior in both computer simulation and field conditions. The results provide evidence supporting the re-evaluation of the default application of the Topp et al., 1980 equation in cryotic soils.

3.1 Introduction

Anthropogenic climate change is fundamentally jeopardizing the stability of ecosystems on a planetary scale (Fussmann et al., 2014). Among the most impacted are polar and sub-polar regions which are warming at up to four times the average global rate, leading to permafrost thaw (Rantanen et al., 2022). Though recent studies have improved our understanding of the impact of permafrost thaw on the local hydrology of specific regions (Jin et al., 2022; Connan et al., 2014), questions remain regarding the exact mechanisms and parameters that control the observed hydrological changes, especially those relating to the hydrologic connectivity of landscape (Walvoord and Kurylyk, 2016). It is well-established that the

presence or absence of frozen soil pore water or segregated ground ice is the dominant control on the connectivity of permafrost landscapes (Connon et al., 2014), but further work is needed to understand the role soil ice content plays on surface water and groundwater movement (Lemieux et al., 2024; Walvoord and Kurylyk, 2016). Flow through frozen soil is controlled by Soil Freezing Characteristic Curves (SFCCs) which describe the relationship between volumetric unfrozen water content ($\theta_{unfrozen\ water\ content}$ or θ_{uwc}) in soils with their Temperature (T).

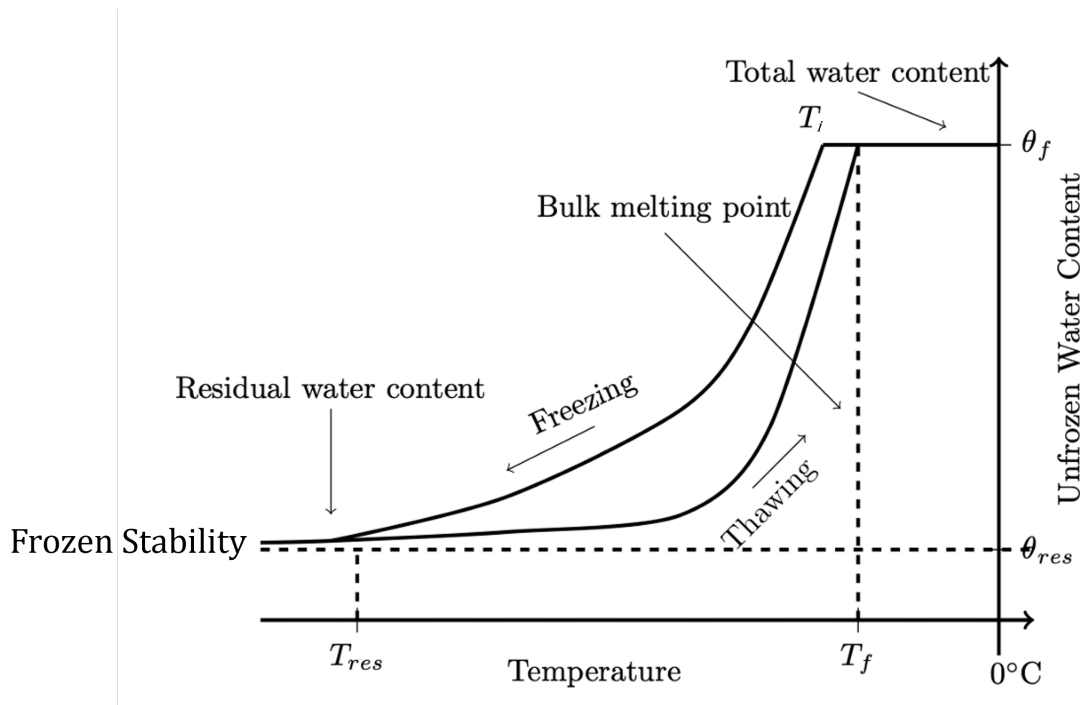


Figure 3.1: Idealized representation of a Soil Freezing Characteristic Curve modified from Devoie et al. (2022).

Sections of notable interest in any SFCC are: the initial total water content θ_f , the first trigger of ice nucleation T_i , the bulk melting point T_f , the residual unfrozen water content θ_{res} and the temperature range of the Frozen Stability region as seen in Figure 3.1. The

initial total water content θ_f is the initial, fully thawed water content of the soil and has been an ongoing source of debate within the scientific community as a controlling parameter of residual water content θ_{res} (Suzuki, 2004; Williams, 1964). The first trigger of ice nucleation T_i represents the temperature associated to the first major event of ice formation of the system. The bulk melting point T_f is the temperature at which the system has fully thawed after a freezing event. The residual unfrozen water content θ_{res} (or in this paper $\theta_{unfrozen\ water\ content}$) is the amount of water that remains in a liquid state even when the system reaches frozen stability at very low temperatures. The frozen stability region is the range of temperature T_{res} for which the unfrozen water content remains at a stable plateau. The freezing point of water is well known to be at 0°C, but SFCCs frequently display T_i that are substantially below this point and elevated amounts of θ_{uwc} even at very low temperatures. These two phenomenon, namely the depression of the freezing point of water and the residual unfrozen water content, are two unusual properties of water which show up in SFCCs and hold considerable value for cold region scientists.

Assessing the unfrozen water content in cryotic soil is challenging: all existing measurement techniques are indirect, like time domain reflectometry (TDR), nuclear magnetic resonance (NMR), calorimetry, and capacitance. In each of these indirect measurement techniques, a conversion curve is required to transform measured values (e.g. capacitance, permittivity, voltage) into unfrozen water content, and current literature does not provide conclusive evidence for the optimal conversion to be applied (Dyck et al., 2019; He et al., 2016; Lijith et al., 2021). Regardless of the precision and accuracy of one's apparatus, if the conversion curve is lacking, so are the data reported. In addition, current measurements from field and

lab settings show poor agreement for identical soil textures, pointing to a need for systematic soil preparation and measurement techniques (Devoie et al., 2022). Given the low cost and ease of installation and maintenance, field and laboratory researchers frequently opt for capacitance based sensors.

Capacitance-based sensors measure the ability of the soil to hold an electrical charge, measured as dielectric permittivity (ϵ). The current default conversion curve used in most commercially available sensors is the Topp et al. 1980 equation which is an empirical third-degree polynomial fit obtained from pooled wetting-drying experimental data (Topp et al., 1980):

$$\theta_{water} = 4.3 * 10^{-6}\epsilon^3 - 5.5 * 10^{-4}\epsilon^2 + 2.92 * 10^{-2}\epsilon - 5.3 * 10^{-2} \quad (3.1)$$

where ϵ is the dielectric permittivity of the soil and θ_{water} is the volumetric water content. Fitting this third-degree polynomial yields a uniformizing behavior on soils that are largely physically distinct from one another. There is no mechanism in this relation to fine tune the conversion curve for specific soils as the fitting parameters are empirical and unrelated to the soil sample characteristics, and the same fitting parameters are used by default unless a soil-specific calibration is performed for each new soil type measured. Most importantly, this empirical fit is intended for use in wetting and drying thawed soils: it has been extended beyond its temperature domain when used in cryotic conditions ($<0^\circ C$) and lacks the capacity to represent phase change.

An alternative to the Topp, 1980 conversion curve is a dielectric mixing model. These models use weighted averages to express the effective dielectric properties of a representative elementary volume (REV) as a function of the proportion of its constituents. Complexity arises once other properties of the constituents such as their geometry, orientation, dielectric contrast with their environment, or depolarization axes are considered (Sihvola, 2000; Jin et al., 2022).

The objective of this paper is to develop an alternative and physically grounded conversion curve for capacitance-based sensors using a multiphase dielectric mixing model. The soil dielectric permittivity mixing model will encompass soil parameters that allow for an adaptable conversion curve tailored to each soil, without the need for soil-specific calibration. Specific attention is given to use parameters that are readily available and well documented in the literature such as porosity ϕ (v/v), bulk density ρ_b , and specific surface area A_s so that soil-specific parameterization is favoured. This paper does not aim to generate a predictive model for SFCCs but rather improve the mathematical conversion of field and laboratory dielectric permittivity measurements into an estimate of volumetric water content.

3.2 Methods

To address the lack of existing physics-based conversion curve for capacitance-based water content sensors, a new conversion curve was developed. This curve is based on dielectric mixing models for thawed, unsaturated soils present in the literature (Sihvola and Alanen, 1991; Sihvola, 2000). This model is refined for use in cryotic soils considering the volume change of water as it undergoes phase change, the temperature-dependence of the dielectric

permittivity of water, and the interactions between the soil, liquid water, and ice phases. The final model obtained through this process is then applied in a laboratory study of several silica samples of varying grain sizes.

3.2.1 Fully Saturated 3 Phase Mixing Model

The baseline used to formulate the mixing model in this paper is the Sihvola Multiphase Mix Model, presented in equation 3.2 (Sihvola, 2000). This model is based on an heterogeneous formulation of the Maxwell Garnett formula which ends up giving a representative value of dielectric permittivity ϵ_{eff} to a multiphase system composed of n phases in a background phase called the “environment” e . The system is composed of uniformly round particles made of phase n which are randomly scattered in orientation and space within background e , as depicted in Figure 3.2. The advantage of the Sihvola Mixing model is

$$\epsilon_{eff} = \epsilon_e + 3\epsilon_e \frac{\sum_{n=1}^N \theta_n \frac{\epsilon_n - \epsilon_e}{\epsilon_n + 2\epsilon_e}}{1 - \sum_{n=1}^N \theta_n \frac{\epsilon_n - \epsilon_e}{\epsilon_n + 2\epsilon_e}} \quad (3.2)$$

Adapting the Sihvola multiphase mix model (equation 3.2) to the idealized soil system in Figure 3.2, we obtain equation 3.3:

$$\epsilon_{eff} = \epsilon_w + 3\epsilon_w \frac{\theta_i \frac{\epsilon_i - \epsilon_w}{\epsilon_i + 2\epsilon_w} + \theta_s \frac{\epsilon_s - \epsilon_w}{\epsilon_s + 2\epsilon_w}}{1 - (\theta_i \frac{\epsilon_i - \epsilon_w}{\epsilon_i + 2\epsilon_w} + \theta_s \frac{\epsilon_s - \epsilon_w}{\epsilon_s + 2\epsilon_w})} \quad (3.3)$$

In this relation, the background phase w is the “unbound water” or pore water (Figure 3.2: blue), the first inclusion phase is ice, i , (Figure 3.2: cyan) and the second inclusion phase

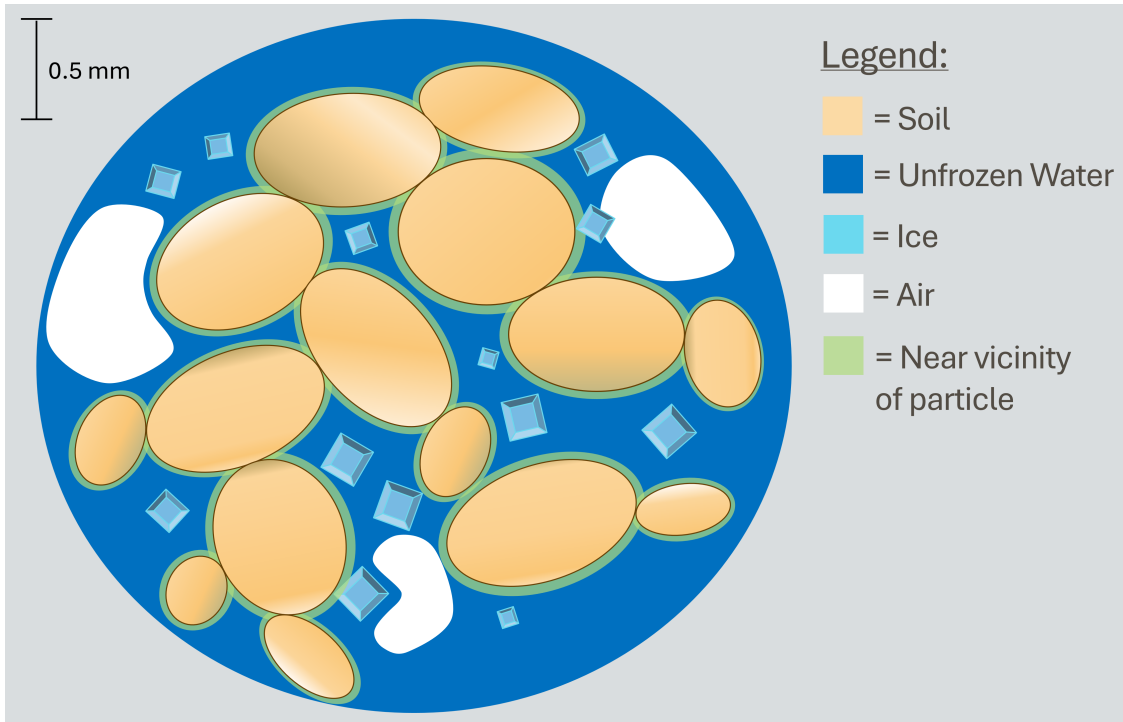


Figure 3.2: Schematic representation of a soil sample in cryotic conditions. The Sihvola Multiphase Mix Model can be adapted to represent the soil sample in an environment, e , of liquid water in which the other phases exist. Note that while ice and air phases are not depicted as round for ease of visualization, they are only mathematically represented as such.

encompass the solid component of soil, s , (Figure 3.2: ochre). ϵ_k here represents the dielectric permittivity of the respective phases $k = i, w, s$, theta θ_k its volume fraction of these phases and ϵ_{eff} is the measured dielectric permittivity of the sample. It is assumed that the medium is fully saturated, and the air phase was omitted in this first formulation for simplicity. The strongly bound water content (Figure 3.2: green) is described in Section 3.2.4 to parametrize the dielectric permittivity of the unfrozen water phase in the near vicinity of soil particles.

3.2.2 Volume Correction for Expansion of Ice

The multiphase complex dielectric model (eq. 3.3) aims to represent ϵ_{eff} of the medium based on the proportion of each phase in the REV. In wetting-drying experiments, no volume expansion takes place, however, water expands in volume by about 10% when it freezes. The multiphase dielectric model is therefore volume corrected as ice forms and thaws. A few assumptions made: all phases are incompressible, including the soil phase, and all the volume expansion is captured by an increase in relative pore space as the pressure exerted by the freezing and expanding ice forces the pores open. The proportion of our system represented by pore space (ϕ_p) is correlated to the portion of our system composed of water (ϕ_w) and ice (ϕ_i). Conservation of mass (m_{wp}) of the water phases (water and ice) results in the argument:

$$m_{wp} = 1.0 * V_w + 0.91 * V_i \quad (3.4)$$

Using equation 3.4 in our definition of the pore space, we can redefine ϕ_i and ϕ_s and sub them into our model from equation 3.3 to get:

$$\epsilon_{eff} = \epsilon_w + 3\epsilon_w \frac{\left(\frac{\frac{m_{wp}-V_w}{0.91}}{V_s+V_w+\frac{m_{wp}-V_w}{0.91}} \right) \frac{\epsilon_i-\epsilon_w}{\epsilon_i+2\epsilon_w} + \left(\frac{V_s}{V_s+V_w+\frac{m_{wp}-V_w}{0.91}} \right) \frac{\epsilon_s-\epsilon_w}{\epsilon_s+2\epsilon_w}}{1 - \left(\frac{\frac{m_{wp}-V_w}{0.91}}{V_s+V_w+\frac{m_{wp}-V_w}{0.91}} \right) \frac{\epsilon_i-\epsilon_w}{\epsilon_i+2\epsilon_w} + \left(\frac{V_s}{V_s+V_w+\frac{m_{wp}-V_w}{0.91}} \right) \frac{\epsilon_s-\epsilon_w}{\epsilon_s+2\epsilon_w}} \quad (3.5)$$

Equation 3.5 now represents volume expansion due to freezing and is dependent on V_w with ϵ_w , ϵ_i , ϵ_s , m_{wp} and V_s as constants. Since full saturation is assumed, the porosity ϕ (v/v) is used to assess the upper boundary of maximum unfrozen water content ($\phi = V_{w\ max}$ i.e. V_w

when the system is fully thawed since it is saturated).

3.2.3 Adaptive Dielectric of Water Phase

For capacitance-based sensors in freezing systems, a measurable decrease in dielectric indicates the nucleation of ice within a sample because the dielectric permittivity of pure water is 80.00 while the dielectric of ice is 3.00 (Evans, 1965; Malmberg and Maryott, 1956). Various conversion curves have been modeled and used to correlate dielectric permittivity to volumetric water content for TDR measurements of SWCCs (Dyck et al., 2019; Topp et al., 1980; He et al., 2016). In these models, it is noted that phenomena other than phase change can lower the dielectric permittivity of the water phase of a sample including the impact of weakly and strongly bound water and temperature on measured permittivity. These controls were modeled as an adaptive dielectric value for the water phase, $\epsilon_{water} = f(\theta_{bound\ water}, T)$, a function of the ratio of bounded water to free water ($\theta_{bound\ water}$) and temperature, T. For $T < 0^{\circ}C$, the theory presented by Bruggeman is used here to describe the evolution of the dielectric of the water phase as pore water, weakly and strongly bound water, freezes, yielding (Malmberg and Maryott, 1956; He et al., 2016; Jin et al., 2020):

$$\frac{V_{bound\ water}}{V_{free\ water}} = 1 - \frac{\epsilon_2 - \epsilon_{mix}}{\epsilon_2 - \epsilon_1} \left(\frac{\epsilon_1}{\epsilon_{mix}} \right)^{\frac{1}{3}} \quad (3.6)$$

where $\epsilon_1 = \epsilon_{free\ water}$, $\epsilon_2 = \epsilon_{bound\ water}$ and $\epsilon_{mix} = \epsilon_{mix\ water}$. Note that the ϵ_{mix} or $\epsilon_{mix\ water}$ is the value used in Eq. 3.5 for ϵ_w during the iterative solving process (See Appendix B for clarification). In this simplified model, strongly bound water only occurs surrounding soil grains while the rest of the water phase is deemed free water. The value of ϵ for free water (87.40) was taken from the National Institute of Standards and technology (NIST)

and the value of ϵ for bounded water (9.00) was taken from the modeling work of Jin et al., 2020 (Jin et al., 2020). The dielectric permittivity of water above 0°C is estimated using the third-degree polynomial:

$$\epsilon = 87.740 - 0.40008 * T + 9.398 * 10^{-4}T^2 - 1.410 * 10^{-6}T^3 \quad (3.7)$$

from the work of Malmberg et al., 1956 (Malmberg and Maryott, 1956). Together, these relations can be iteratively solved for ϵ_w in equation 3.5, giving soil-specific results (See Figure 3.3).

3.2.4 Strongly Bound Water Characterization

$V_{\text{bound water}}$ represents the volume of strongly bound water in a soil, correlated to the adsorption force, specific surface area, and electric dipole potential of the soil grains. The Stern-Gouy electrical double-layer theory informs the basic plate model used here (Dobson et al., 1985):

$$\theta_{sbw} = \delta * A_s * \rho_b * 10^{-4} \quad (3.8)$$

where θ_{sbw} is the volume fraction (v/v) of strongly bounded water content, δ is the thickness of the layer of strongly bounded water [\AA], A_s is the specific surface area [m^2/g] and ρ_b is the soil bulk density [g/cm^3]. Note that Eq. 3.8 defines $V_{\text{bound water}}$ used in Eq. 3.6, which remains fixed for a given soil. The δ parameter is kept consistent as 5 \AA , the average representative thickness of strongly bounded water for all studied soils (Jin et al., 2020;

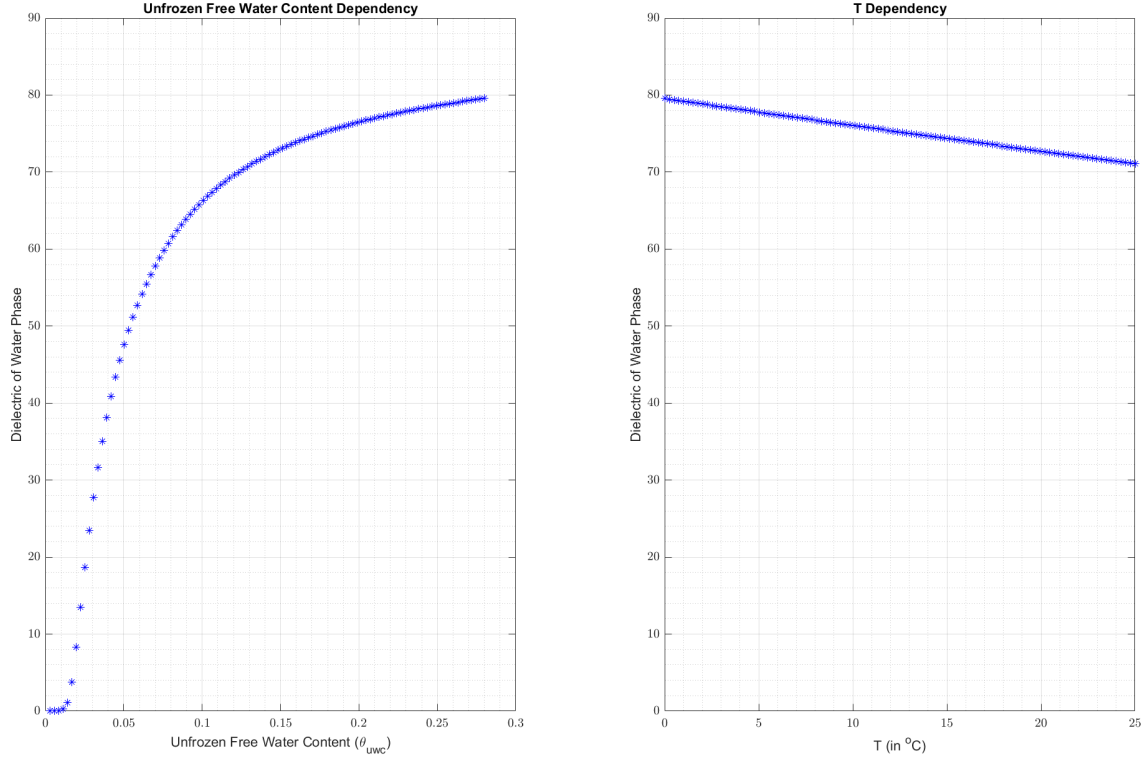


Figure 3.3: Theoretical representation of $\epsilon_{water} = f(\theta_{water}, T)$, the temperature dependence reported in equation 3.7 (Malmberg and Maryott, 1956) is applied for above-zero temperatures (right), and for $T < 0^{\circ}\text{C}$, equation 3.6 is applied (left). This is an example of synthetic data from a soil that would have porosity $\phi = 0.28$ (v/v) and $\theta_{sbw} = 0.02$.

Shang et al., 1994; Olphen, 1964; Verwey, 1947). Details on the numerical algorithm used to solve the system of equation can be found in Appendix B.

3.3 Experimental Method

A set of 6 800 mL glass beakers were filled with soils to 600 mL, three of which were undisturbed natural soils, and three homogeneous, well-characterized silica porous media, as described in Table 3.1 (See Section 3.4). The beakers were saturated with tap water in the case of the natural soils, and deionized (DI) water for the silica. For the washed silica

materials (graded sands and flour) DI water was used, but tap water was used for the natural samples to more closely match the in-situ pore water. A 5TM capacitance sensor was placed in each of the samples to record the dielectric permittivity and Temperature (METER, 2025a). The sensor was inserted vertically from the soil surface, and the prongs were 2.0 cm from the bottom of the beaker. The prepared beakers were covered with parafilm to avoid evaporation/sublimation effects. Special attention was given to keep the field samples (Beaker 1 to 3) undisturbed to retain their original soil pore structure. The samples were then freeze-thaw cycled in a Binder MK56 climate chamber from room temperature (21°C) to -6°C . The reversal point from freezing to thawing was determined to be -6°C because no discernible changes in θ_{uwc} were observed for colder temperatures. The climate chamber was programmed so that the samples would equilibrate at each temperature, maintaining the internal temperature for between 2.0 and 4.0 hours depending on the thermal inertia of the sample, with temperatures near the ice nucleation point requiring significantly longer to equilibrate due to phase change. These samples were subject to 8 temperature cycles in the programmable chamber, from which paired temperature-permittivity data were extracted for the periods when the soils had equilibrated to the internal temperature of the climate chamber. The sensors' accuracy for apparent dielectric permittivity ε_{eff} is reported to be: $\pm 1 \varepsilon$ for the $1\text{--}40 \varepsilon$ range (soil range) but is 15% of the measurement for the $40\text{--}80 \varepsilon$ range (METER, 2025a). The data were also corrected for temperature (T) measurement bias in the 5TM sensors, which have a reported accuracy of $\pm 1^{\circ}\text{C}$ and a resolution of 0.1°C (METER, 2025a). The temperature recorded by the 5TM probes was compared to the temperature set in the climate chamber, and when bias was detected it was corrected, as detailed in appendix C. These data were converted using equation 3.5 to populate a Soil Freezing Characteristic Curve (See Section 3.4. Results, Figure 3.4 and Figure 3.5).

3.4 Results

The raw dielectric readings from the 5TM sensors were input as ϵ_{eff} , alongside the corrected temperature, T from the sensor (see Appendix A), porosity ϕ (v/v), surface area A_s and bulk density ρ_b specific to each sample (See Appendix B). The complete data pre-processing workflow is included in Appendix A and the design of the solver's algorithm is expanded upon in Appendix B. Once transformed, the SFCC relating the θ_{uwc} and temperature was plotted to compare results using the conversion curve suggested here, alongside the default *Topp, 1980* model, shown in figure 3.4.

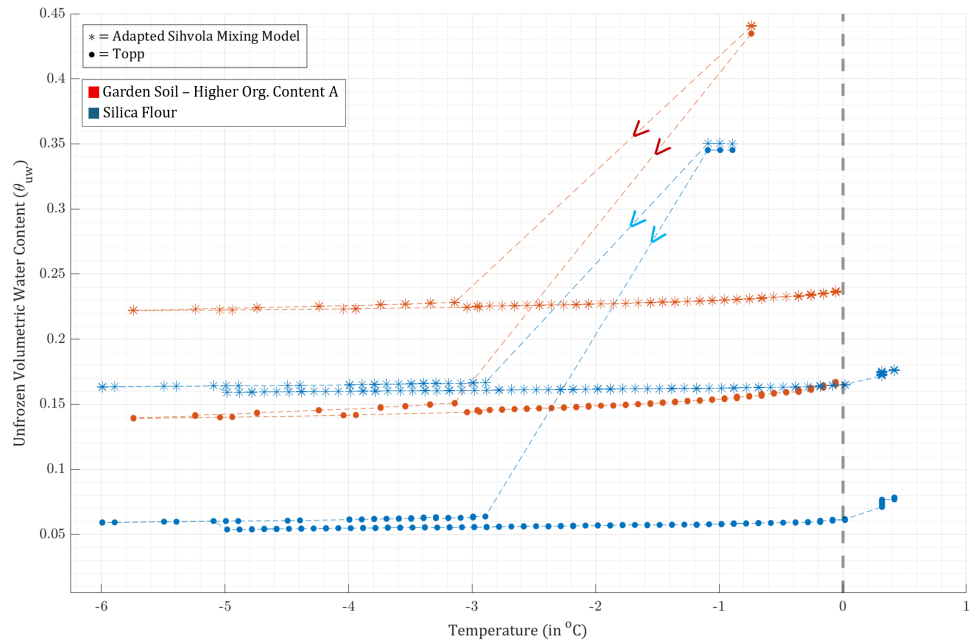


Figure 3.4: Comparison of volumetric unfrozen water content (θ_{uwc}) data for two soils. Both the *Topp, 1980* conversion curve (\bullet) and the multiphase dielectric model (*) developed in this paper are represented. The coloured arrows indicate the direction of the freeze to thaw cycle direction for clarity, where the freezing limb has greater unfrozen water content than the thawing limb for equivalent temperatures.

Figure 3.4 is the result of two combined Freeze-Thaw runs on two samples: Garden Soil –

Higher Organic Content A (red) and Silica Flour (cyan). The data converted using *Topp, 1980* had -8.3% residual volumetric water content (v/v) for the Garden Soil sample, and -10.4% residual volumetric water (v/v) for the Silica Flour compared to the data converted with Eq. 3.5. For this set of data, this represents near 200% error.

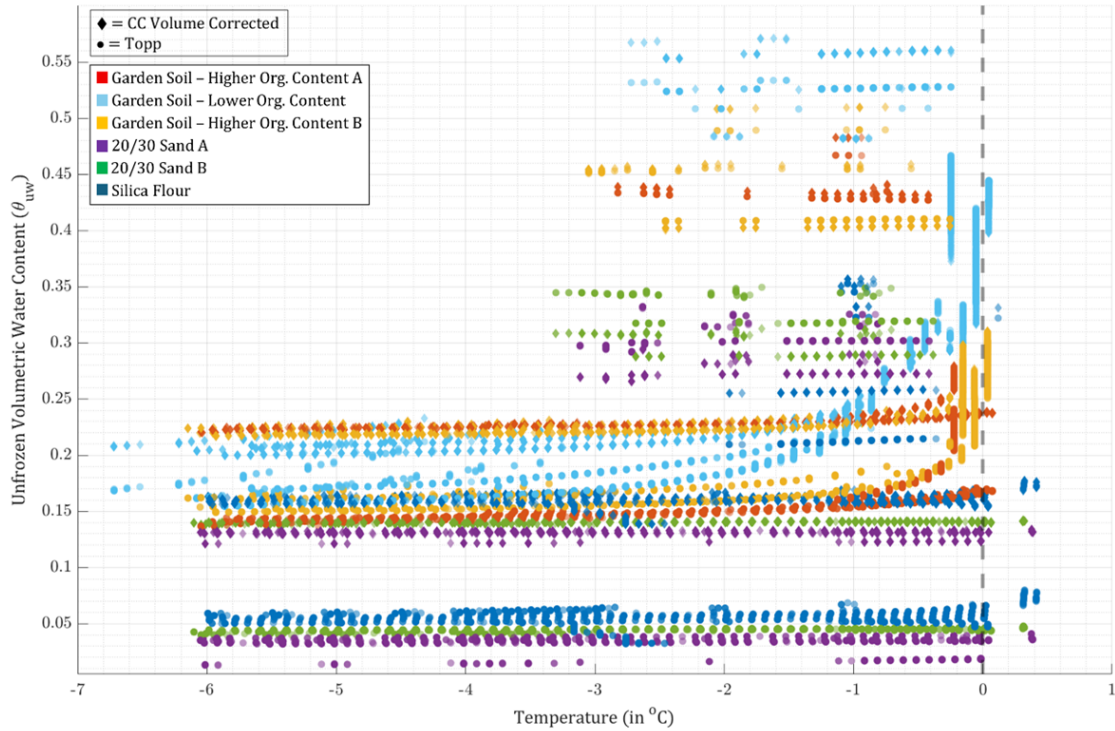


Figure 3.5: Complete dataset of 6 soil types and 8 Freeze-Thaw programs. Both the *Topp, 1980* conversion curve (\bullet) and the multiphase dielectric model (\blacklozenge) developed in this paper are represented.

Figure 3.5 shows the complete set of Freeze-Thaw data and soil samples for each conversion curve, while the difference in residual unfrozen volumetric water content for each sample depending on the choice of conversion curve is included in Table 3.1. Sample 1 to 3 were obtained from the "field" and given special care to conserve their original pore structure and sample 4 to 6 were constructed from bulk soil in the lab. Soil 1-3 were characterized as XXX

Port Number	1	2	3	4	5	6
Soil Type	Garden soil - Higher Org. Content A	Garden soil - Lower Org. Content	Garden soil - Higher Org. Content B	20/30 Sand A	20/30 Sand B	Silica Flour
Water Type	Tap	Tap	Tap	DI	DI	DI
Low T Plateau θ_{uw} (Topp VS Mixing Model)	- 0.080	-0.038	-0.064	-0.097	-0.098	-0.106

Table 3.1: Description of the 6 soils used for Freeze-Thaw experiments, the source of water used, and the change in residual volumetric water content based on the choice of conversion curve. The silica flour has a mean volume size of $60 \mu\text{m}$. Extra metadata about each soil which is necessary to use the mixing model can be found in Appendix B, Table B.1.

using the USDA soil texture triangle (Groenendyk et al., 2015). The greatest discrepancy occurred in the Silica Flour sample at -10.6% (v/v) residual water content and the smallest in the Garden soil - Lower Org. Content sample at -3.8% (v/v).

3.5 Discussion

When compared to data available in the literature, the SFCCs converted with Eq. 3.5 and the Topp et al. (1980) model for two 20/30 sand samples ([purple](#) and [green](#)) reported in figure 3.5 compare well . SFCCs for sandy soil reported in the literature (e.g. Devoie et al. (2022) and Vu et al. (2022)) are quite similar to the ones in Figure 3.5 using the Topp et al. (1980) (\bullet) but (understandably) differ from the one converted with Eq. 3.5 (\blacklozenge). The Topp et al. (1980) data in Figure 3.5 reports very low values of residual θ_{uw} i.e. $< 0.05 \theta_{uw}$ on the frozen stability range for low clay contents sand as do Devoie et al. (2022) and Vu et al. (2022). The Temperature of bulk melting point is also close to the 0°C axis. The SFCCs converted with Eq. 3.5 have much higher residual unfrozen water content that still sit in the upper range of values reported by Devoie et al. (2022). Data converted with Eq. 3.5 also shows frozen stability (no thawing) all the way to the 0°C axis on their thawing limbs. This comparison lends confidence to the data reported, which fall within the upper range of values reported using both capacitance-based sensors and other methods.

3.5.1 Error in parameter estimation

The proposed model has three main input parameters which characterize the soil type: ϕ the porosity (v/v), A_s the specific surface area [m^2/g] and ρ_b the soil bulk density [g/cm^3].

When compared to the Topp model which includes only fitting parameters as input, this introduces a potential source of uncertainty or error in measurement due to incorrect parameter estimation. To constrain the error introduced through parameter estimation, $\pm 10\%$ error margins on the porosity ϕ (v/v), the specific surface area A_s and bulk density ρ_b parameters are presented in Figure 3.6.

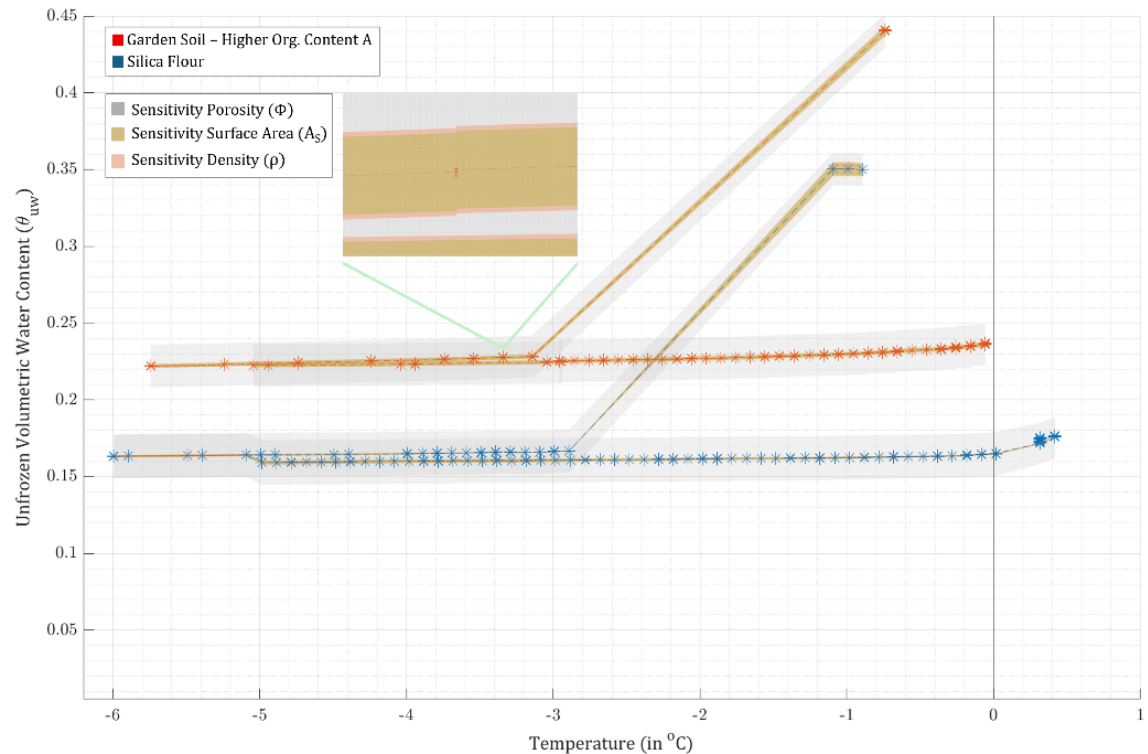


Figure 3.6: Sensitivity analysis on input parameters for the same dataset presented in Figure 3.4. Both the *Topp, 1980* conversion curve (\bullet) and the multiphase dielectric model (*) developed in this paper are represented.

The magnitude of error introduced is independent of temperature for the porosity ϕ (v/v) parameter but exhibits temperature dependence for the surface area A_s and bulk density ρ_b parameters, where measurements in the freezing limb are more sensitive to error, and temperatures close to 0°C have wider error margins. When comparing the sensitivity of the model to each parameter, the reported unfrozen water content is much more sensitive to changes in the porosity (v/v) than other parameters as shown in Figure 3.4. This sensitivity can primarily be ascribed to the assumption that the sample is fully saturated. The reported unfrozen water content is thus much more sensitive to the description of the soil pore structure than to the properties of the soil grains. Though the sensitivity to surface Area A_s and bulk density ρ_b parameters are relatively small, the $\pm 10\%$ perturbation is applied to an already small in magnitude input parameter reported in Appendix B Table B.1. Substantially different values of A_s and ρ_b representing different soil types more notably alter the final θ_{uwc} .

3.5.2 Sensitivity to parameter selection

The input parameters A_s and ρ_b are described in Equation 3.8 and characterize the strongly bound water. Both those variables are multiplicative, so they have the same linear and proportional effect on the θ_{sbw} term. Since the strongly bound water content is the last water to freeze, an increase in θ_{sbw} yields greater residual unfrozen water content (θ_{uwc}) and vice versa. A decrease in $\varepsilon_{mix\ water}$ can be explained by two things: The formation of ice which reduces the proportion of $V_{free\ water}$ or a higher $V_{bound\ water}$ as determined by Eq. 3.8).

The porosity parameter ϕ (v/v) is directly proportional to the residual final unfrozen water content. In Equation 3.6 as $V_{free\ water}$ increases with $V_{bound\ water}$ fixed, the bound water

to free water ratio decreases yielding an overall higher dielectric permittivity value, ϵ_{mix} . This translates to a greater $V_{free\ water}$ as it is the only parameter that can change to explain a change in dielectric (Note: A lower θ_{sbw} i.e. $V_{bound\ water}$ can also explain a higher dielectric but the $V_{bound\ water}$ value is fixed by Equation 3.8). Similarly, a reduction in porosity (v/v), yields a lesser residual θ_{uwv} .

3.5.3 Comparison with Topp

The *Topp, 1980* conversion curve under-estimates the residual unfrozen water content in every soil type analyzed in this paper. The greatest discrepancy is seen in the silica flour -10.6% (v/v), while the Garden soil - Lower Org. Content only showed a -3.8% (v/v) discrepancy. It is likely that this is due to the significant specific surface area (SSA) of the silica flour sample, yielding higher bound water content, while the garden soil had evidence of macropores containing bulk water, better captured by the simpler *Topp, 1980* model. On average, over all soil samples, our results indicate that the *Topp, 1980* conversion curve under-predicts the residual unfrozen water content by 8% (i.e. VWC % values are 8 units lower than they should be). This consistent under-prediction of residual unfrozen water content at low temperature from *Topp, 1980* is concerning as it represents a significant portion of the overall residual unfrozen water content: the residual water content is near tripled when applying Equation 3.5 as a conversion curve.

In addition to a clear consistent discrepancy in residual unfrozen water content, the correction for an adaptive ϵ_{water} and a volume correction for ice volume expansion applied to the model developed in this paper also alters the SFCCs curvature near the bulk melting point.

In figure 3.5, the residual water plateaus can be seen slowly thawing at different temperatures than their *Topp, 1980* counterparts. This shows a different thawing behavior where small changes of dielectric in intermediate freezing temperatures do not necessarily correlate to a phase change from solid ice to unfrozen water, but rather a change in ε_{water} based on the θ_{water} and T dependent relationship presented in Figure 3.3. The lower organic content garden soil sample (*cyan* in Figure 3.3) reaches a similar final state of frozen stability zone (low-end temperature plateau), but the curvature of the data set (formation of first onset of ice nucleation) is less steep with a greater freezing point depression than the higher organic content soils (*red* and *ochre* in Figure 3.3) which starts curving closer to 0°C. This is consistent with organic content promoting the heterogeneous nucleation of ice and the greater proportion of macropore space which lessens the level of supercooling the sample would undergo (Head, 1961; Fukuta and Mason, 1963; Pummer et al., 2015).

3.5.4 Impact of under-estimating unfrozen water content in freezing soils

Having a residual water content three times greater than the *Topp, 1980* prediction yields notably different latent heat exchange for both the freezing and thawing limb of the SFCC. Since the nucleation of ice is an exothermic process and the thawing of ice is an endothermic process, phenomenon such as the “0°C curtain effect” is apparent for the first major nucleation events (See Figure C.1 for an example) (Outcalt et al., 1990). Because *Topp, 1980* over-predicts the ice formed (under-predicts the unfrozen water content), it would yield a greater release of latent heat and a more pronounced 0°C curtain effect in a predictive heat transfer model such as GeoStudio.

Unfrozen water content greatly impacts the thermal-hydro-mechanical properties of frozen

soil, and a 200% error could lead to dramatic change in expected behavior in both computer simulation and field applications (Fisher et al., 2019). For example, hydraulic permeability is a key physical property of soils for contaminant transport and remediation (Li et al., 2019; Wu et al., 2024). Hydraulic permeability strongly depends on θ_{uwc} and decreases exponentially with decreasing temperature (Kleinberg and Griffin, 2005; Watanabe and Osada, 2017).

Another field impacted by θ_{uwc} is infrastructure stability and longevity. Strength properties of soils are frequently expressed as a function of their total moisture content and exponential relationships between unfrozen water content and peak strength of saturated sandstone shows a good relationship in recent scientific publications (Li et al., 2025; Shusherina et al., 1978). The less ice and more unfrozen water there is in soil, the less cohesive it is and the easier to strain or break it becomes. This is particularly apparent in the proportional increase of minimum creep strain rate with increasing unfrozen water content and the decrease of adfreeze bond strength with increasing water content (Arenson and Springman, 2005; Sun et al., 2021). The adfreeze strength often referred to as “grip” is the ability of ice rich soil to “hold” onto foundations piles, a property which decreases the more thawing a soil undergoes due to the significant increase in unfrozen water content during the thawing process (Alqaed and Rayhani, 2019). Landslide initiation processes in Nordic regions have also been increasingly linked to permafrost thaw, especially due to the loss of cohesion and friction associated with the loss of ice (Walvoord and Kurylyk, 2016; Patton et al., 2021).

3.5.5 Sources of error

Though an improvement over the *Topp 1980* model in cryotic soils, there are still several sources of error present in the measurement and conversion proposed here. In the results here, despite a higher SSA parameter, the silica flour has a lower residual unfrozen water content than the Garden Soil. Known parameters influencing greater residual unfrozen water contents include the presence of solutes in the pore water and the amount of adsorptive and capillary water, the later being predominantly governed by clay content of the studied soil (Dillon and Andersland, 1966; Resurreccion et al., 2011). The higher the clay content, the higher adsorptive and capillary water. However, other phenomenon like partitioning solute effects may also affect residual unfrozen water content. As ice crystalizes, solutes are preferably partitioned into the liquid phase of water rather than the solid phase. This causes solute concentrations to rapidly climb in the liquid phase as freezing occurs, lowering the freezing point depression. Since the Garden Soil sample is a field sample, solutes are inherently present, derived from organics (nutrients), leached off specific mineral phases (bedrock, evaporite, carbonate etc...) or from intrusions (seawater, rain, pesticides, sewer water, mine tailings etc...) (USGS, 2016; Nambu et al., 2008; Warren and Spiers, 2021). A study of the exact nature of the ionic content and microbial activity in the sample would be required to completely assess their impact on nucleation potential as their impact varies based on hydration effects, namely the orientation and molecular bonding of water molecules (Ding et al., 2019). The Garden Soil sample may also retain higher unfrozen water content because organic matter can be hydrophilic (i.e. high ability to bind water) and have extensive SAA (Leelamanie and Karube, 2009). Additionally, organic matter is a dual porosity (v/v) material, where smaller dead-end or disconnected pores within the organic matter (OM) itself bind and hold water (Cates, 2020; Delle Piane et al., 2022). This

has been demonstrated in medium-textured soil, where increasing OM by 1% leads to an increase in water content of 1.03% (Maeda, 2021; Minasny and McBratney, 2017). Further characterization of the exact nature of the OM in soil samples would further constrain its impact on θ_{uwc} . Lastly, the dielectric permittivity of organic content is itself very low ([2.0-3.0]) and would increase the impact of the ϵ_s parameter, lessening the requirement of ice content to explain the low dielectric readings (Sami et al., 2022; Yang et al., 2024).

A source of error with the potential to yield an under-estimate of unfrozen water content is the suspension of the clay or other fines present in saturated soils. Not only are the total dissolved solids (TDS) in pore water indicative of its physical and electrical properties but so is the amount of its total suspended solutes (TSS). The impact and parametrization of suspended fines in pore water is tackled in modern civil engineering challenges surrounding the longevity and safety of heavy-haul tracks and other industrial transportation infrastructures (Indraratna et al., 2020; Wan et al., 2022). The presence of colloids within the water phase would make the actual ϵ_{mix} lower and force the solving algorithm towards creating more ice to lower the ϵ_{mix} . If deemed a substantial factor, an added factor of ϵ_3 involving fluidized fine should be added to Equation 2.4 to palliate for the bias. On the other hand, depending on the nature of the fines, they may act as heterogeneous nucleation sites within the free water phase and promote ice nucleation, lessening supercooling (Maeda, 2021). The impact of fluidized fines in the liquid phase demands further inquiries before a conclusive answer on their impact can be stated.

3.5.6 Limitations in the applicability of the conversion curve

The multiphase dielectric mixing model developed in this paper was developed with the capacitance measuring technique in mind. That is, it works on the principle that the capacitance of the sample varies due to the phase change of water, something which is captured in its apparent dielectric permittivity. However, measurement techniques for θ_{uwc} in cryotic soils, despite all needing some sort of conversion curve, are quite varied in the principles underlying the detection and quantification of unfrozen water content. Capacitance, treats the soil as a capacitor and analyzes the time it takes for it to hold a certain electric charge which is indicative of its dielectric permittivity ϵ_{eff} . Time Domain Reflectometry (TDR) on the other hand uses interference and reflection patterns of an electrical signal in a conductor to infer impedance changes in its surroundings. A similar dielectric mixing model is needed to convert ϵ_{eff} to θ_{uwc} but is dependent on the real and imaginary part of ϵ_{eff} as well as the frequency f of the signal. The dielectric mixing model developed in this paper is restricted to application in capacitance-based measurements but recent work like Dyck et al., 2019 include strongly bounded water and dual porosity in their conversion model for TDR measurements.

The strength of the capacitance-based sensors used here is their applicability in the field. However, the analysis presented thus far is limited to saturated systems, therefore for the analysis of field data, additional work should be done on the mixing model to encompass a fourth gas (air) phase and extend the conversion process to unsaturated soils. The laboratory setting described in this study establishes volumetric unfrozen water content for specific temperatures in equilibrium conditions, which are not guaranteed in a field setting. The weather drives the temperature of the soil according to heat propagation equations,

resulting in characteristic “trumpet curve” plots all year round, and temperature gradients leading at best to quasi-equilibrium conditions (Romanovsky et al., 2010). Rarely is the temperature recorded by sensors at depth in equilibrium with air temperature, and so most phase changes occur in disequilibrium conditions throughout the freeze-thaw cycle. Selection criteria should be reworked to better capture near-equilibrium state data points in field conditions (See Appendix A). Signal analysis methods using cross-correlation, convolution and derivative analysis would help categorize points of interest to retain, especially in the $\frac{dT}{dt}$ space i.e. the change of temperature T by time t. Because soils in field settings cannot be guaranteed to ever reach thermal equilibrium with their surroundings due to near constantly evolving boundary conditions, the definition of points to be kept in the "EQ point" picking of the pre-processing workflow (See Appendix A) would need to be reworked to "near thermal equilibrium" conditions rather than perfect thermal equilibrium. A plausible and satisfactory picking criteria could be low values of $\frac{dT}{dt}$ and/or reversal points. Additional complications involving change in boundary condition such as wind speed (evapotranspiration), snow cover and even vegetation cover may further complicate the characterization of points to be retained to appropriately convert through the mixing model.

In future work, it would be beneficial to compare “true” versus predicted measurements of unfrozen volumetric water content to better validate the accuracy of both conversion methods. Investigation of pore water ionic and organic content would further help the precision and accuracy of Equation 3.6. The importance of an improved mixing model that encompass a more accurate depiction of weakly bounded water could also further benefit this conversion model.

3.6 Conclusion

A new conversion curve for the interpretation of raw dielectric measurements of unfrozen water content in cryotic soils is presented. The relation relies on the characterization of a soil sample's dielectric permittivity as a multiphase heterogeneous system using physical sample characteristics including specific porosity ϕ (v/v), surface area A_s and bulk density ρ_b . The benefit of using this conversion curve is that the mixing model is both adaptable to soil types and developed with cryotic conditions in mind. Our results highlight that the default conversion used in most capacitance-based instruments namely the *Topp, 1980* equation dramatically under-predicts the residual unfrozen water content at low temperature on average by 8% v/v, regardless of soil type. In the entire dataset, this was seen to be as high as 10.6% v/v for the Silica Flour sample and as low as 3.8% v/v for the Garden Soil – Lower Organic Content sample. The implications of this under-estimate are discussed alongside recommendations regarding the use of this conversion curve.

3.7 Data Availability

The complete set of code necessary for the entire pre-processing (Appendix A) and conversion of raw dielectric permittivity ϵ into θ_{water} using the conversion curve developed in this paper (Eq. 3.5) can be found in an open source repository here. The code consists of 2 MATLAB scripts, part 1 does the pre-processing (See Appendix A) of the data and part 2 the actual conversion (See Appendix B) of ϵ_{eff} into θ_{uwc} .

Chapter 4

Conclusions and Recommendations

4.1 Conclusions

The primary objective of this research was to create a new empirically grounded conversion curve for the capacitance method of measuring unfrozen water measurements in cryotic soils. This thesis presents the new conversion curve from dielectric permitivity to unfrozen water content, but also provides comprehensive tools for researchers to apply the new conversion curve to their own data. The primary contribution (Chapter 3) describes the derivation of the conversion curve as it is based on soil physics and thermodynamics and reports the difference between the conventional conversion curve (Topp et al. (1980)) and the new model. The study assessed the efficacy of these two conversion curves using a freeze-thaw lab experiment considering field and laboratory soil samples. The following conclusions can be drawn from this investigation:

- The current most widely used conversion curve for soil moisture measurements (Topp et al. (1980)) in cryotic soil is inadequate. The *Topp, 1980* model fails to account for i) frozen conditions, ii) phenomenon regarding the phase change of water to ice, and iii) lacks transferability between soil types. The issues with the current conversion

curve (Topp et al. (1980)) are described in Section 2.6.1 and Section 3.1.

- The current state of knowledge regarding multiphase dielectric mixing model is transferable to soil science. A review of current literature regarding dielectric mixing models is provided to assess the current state of knowledge of describing the ϵ_{eff} of multiphase heterogeneous systems. A simplified model from Sihvola (2000), originally describing the theoretical representation multiphase mixtures with uniform spherical components (equal 3-dimensional depolarization factors) that are randomly oriented in space, is adapted (Section 3.2) to cryotic soil systems. The rationale as well as the ice expansion correction (not included in the simplified model) are presented.
- Soil specific parameters used in Eq. 3.5 to characterize the physical properties of soils impact θ_{uwc} (Figure 3.6) consistently with theory reported in literature. The conversion curve is solved following the methodology outlined in Appendix B, and the model (Eq. 3.5) is described in Section 3.5.1. In addition, the degree of bias/error propagation of each parameter required to solve the system of equations (Eq. 3.5 and Equation 3.6 is presented in Section 3.5.1.
- The difference between the conventional conversion curve (Topp et al. (1980)) and the newly developed model (Eq. 3.5) is presented in Section 3.4. This section highlights that the *Topp, 1980* model dramatically under-reports the residual θ_{uwc} by a factor of 200% i.e. the value of θ_{uwc} is nearly three time as small as the value reported using Eq. 3.5. This is especially apparent for the low Temperature frozen stability part og the SFCCs.
- Several other fields use θ_{uwc} to i) make enlightened decisions regarding the design

of infrastructure in permafrost regions or ii) use θ_{uwc} as a parameter in their numerical models. The impacts of such dramatic under-representation of residual θ_{uwc} (200% error) at low temperatures dramatically alters the estimation of thermal-hydro-mechanical properties of the soil. In either field or numerical applications, this can lead to different and potentially hazardous soil and hydraulic behavior (See Section 3.5.4).

4.2 Contributions

This work has revealed significant uncertainty regarding existing methods for the conversion of raw dielectric permittivity measurements to θ_{uwc} . The contributions of this thesis to the broader engineering and scientific community are as follow:

- A dielectric mixing model (conversion curve) was developed for the accurate conversion of measured dielectric permittivity to unfrozen water content in freezing saturated soils. This curve is transferable to different soils through altering soil-specific parameters ϕ porosity (v/v), A_s specific surface area [m^2/g] and ρ_b soil bulk density [g/cm^3]. This allows the Conversion Curve Equation 3.5 to provide soil-specific results. The parameters used here are metadata readily available to field and laboratory measurements and are widely reported in the literature.
- The complete set of experimental data used and produced for this thesis is shown in Figure 3.5 and is available for use here.
- Clarifications about the pre-processing workflow on the raw dielectric value reported by widely used 5TM sensors is presented in Appendix A. This section presents the Temperature T correction for instrument bias, and filters the equilibrated data.

- The mathematical algorithm used to solve the system of equations required to use Eq. 3.5 is presented in Appendix B. This section presents the design of the solver, reports the parameters used for the data transformed in this paper, and describes the iterative solver.
- The complete set of MATLAB code for i) the pre-processing of raw data and ii) the conversion using the newly developed model is provided here.

4.3 Limitations and Recommendations

The limitations of the developed models regarding i) which measurement methods it is compatible with and ii) what type of data it is applicable to are tackled in Section 3.5.6. Future improvements on i) the mixing model (Eq. 3.3) and the ii) pre-processing workflow (Appendix A) are presented. These limitations are:

- Despite having a greater SSA, the silica flour shows lower residual θ_{uw} than the Soil Garden symbol. Note that this is also true when using the *Topp, 1980* model. This highlights several phenomenon not captured in Eq. 3.5 that may further impact residual θ_{uw} and may need to be accounted for in future iterations of the model (Section 3.5.5).
- The model developed in this thesis (Eq. 3.5) can only be applied to the Capacitance measurement method, not the TDR or NMR method.
- The model (Eq. 3.5)) lacks a fourth "air" phase that would extend the range of use to unsaturated system. This is required for the application of this model to general field measurements. This would also prompt a reworking of the "Ice Expansion" correction of Eq. 3.5.

- In Appendix A, the assumption that the system will eventually reach thermodynamical equilibrium is used to assess i) the instrument-consistent temperature bias and ii) equilibrium points. This assumption does not hold in the field as temperature fluctuations are continuous and unpredictable, meaning that a new "near equilibrium point" finding algorithm would be required to apply Eq. 3.5 to field data.

Bibliography

- Aldaeef, A. A. and Rayhani, M. T. (2019). Interface shear strength characteristics of steel piles in frozen clay under varying exposure temperature. *Soils and Foundations*, 59(6):2110–2124.
- Allagui, A., Benaoum, H., and Olendski, O. (2021). On the gouy–chapman–stern model of the electrical double-layer structure with a generalized boltzmann factor. *Physica A: Statistical Mechanics and its Applications*, 582:126252.
- Anderson, D. M. and Morgenstern, N. R. (1974). Physics, chemistry, and mechanics of frozen ground. a review : Conference. in permafrost - north american contribution to the 2nd internat. conference. *International Journal of Rock Mechanics and Mining Sciences & Geomechanics Abstracts*, 11.
- Anderson, D. M. and Tice, A. R. (1972). Predicting unfrozen water contents in frozen soils from surface area measurements. *U.S. Army Cold Regions Research and Engineering Laboratory*.
- Arenson, L. U. and Springman, S. M. (2005). Mathematical descriptions for the behaviour of ice-rich frozen soils at temperatures close to 0 °c. *Canadian Geotechnical Journal*, 42(2):431–442.

- Atkins, P. and De Paula, J. (2006). Physical Chemistry for the Life Sciences. *Oxford University Press*.
- Baker-Fales, M., Gutiérrez-Cano, J. D., Catalá-Civera, J. M., and Vlachos, D. G. (2023). Temperature-dependent complex dielectric permittivity: a simple measurement strategy for liquid-phase samples. *Scientific Reports*, 13(1).
- Bertotti, G. and Mayergoyz, I. D. (2014). The science of hysteresis. *Academic Press Vol. 13*.
- Bhavya, K. and Nagaraj, H. B. (2025). Influence of soil structure and clay mineralogy on atterberg limits. *Scientific Reports*, 15(1):15459.
- Birchak, J., Gardner, C., Hipp, J., and Victor, J. (1974). High dielectric constant microwave probes for sensing soil moisture. *Proceedings of the IEEE*, 62(1):93–98.
- Biskaborn, B. K., Smith, S. L., Noetzli, J., Matthes, H., Vieira, G., Streletskeiy, D. A., Schoeneich, P., Romanovsky, V. E., Lewkowicz, A. G., Abramov, A., Allard, M., Boike, J., Cable, W. L., Christiansen, H. H., Delaloye, R., Diekmann, B., Drozdov, D., Etzelmüller, B., Grosse, G., Guglielmin, M., Ingeman-Nielsen, T., Isaksen, K., Ishikawa, M., Johansson, M., Johannsson, H., Joo, A., Kaverin, D., Kholodov, A., Konstantinov, P., Kröger, T., Lambiel, C., Lanckman, J.-P., Luo, D., Malkova, G., Meiklejohn, I., Moskalenko, N., Oliva, M., Phillips, M., Ramos, M., Sannel, A. B. K., Sergeev, D., Seybold, C., Skryabin, P., Vasiliev, A., Wu, Q., Yoshikawa, K., Zheleznyak, M., and Lantuit, H. (2019). Permafrost is warming at a global scale. *Nature Communications*, 10(1):264.
- Boutoucos, G. (1921). A new classification of the soil moisture. *Michigna Agricultural Station*, XI, No 1:33–48.

- Bruggeman, D. A. G. (1935). Berechnung verschiedener physikalischer konstanten von heterogenen substanz. i. dielektrizitätskonstanten und leitfähigkeiten der mischkörper aus isotropen substanz. *Ann. Phys.*, 416(7):636–664.
- Callaghan, P., Dykstra, R., Eccles, C., Haskell, T., and Seymour, J. (1999). A nuclear magnetic resonance study of antarctic sea ice brine diffusivity. *Cold Regions Science and Technology*, 29(2):153–171.
- Cameron, I. L., Hunter, K. E., Ord, V. A., and Fullerton, G. D. (1985). Relationships between ice crystal size, water content and proton NMR relaxation times in cells. *Physiol Chem Phys Med NMR*, 17(4):371–386.
- Cates, A. (2020). The connection between soil organic matter and soil water. <https://water.unl.edu/article/animal-manure-management/connection-between-soil-organic-matter-and-soil-water/>.
- CGU (2025). Permafrost 101. <https://canadianpermafrostassociation.ca/What-is-Permafrost.htm>. *Canadian Geophysical Union*.
- Chaplin, M. (2021). Hexagonal ice (ice ih).
- Cihan, A., Birkholzer, J., Illangasekare, T. H., and Zhou, Q. (2014). A modeling approach to represent hysteresis in capillary pressure-saturation relationship based on fluid connectivity in void space: A modeling approach to represent hysteresis. *Water Resources Research*, 50(1):119–131.
- Connon, R. F., Quinton, W. L., Craig, J. R., and Hayashi, M. (2014). Changing hydrologic connectivity due to permafrost thaw in the lower liard river valley, nwt, canada. *Hydrological Processes*, 28(14):4163–4178.

- de Loor, G. P. (1968). Dielectric properties of heterogeneous mixtures containing water*. *Journal of Microwave Power*, 3(2):67–73.
- Delle Piane, C., Ansari, H., Li, Z., Mata, J., Rickard, W., Pini, R., Dewhurst, D. N., and Sherwood, N. (2022). Influence of organic matter type on porosity development in the wufeng-longmaxi shale: A combined microscopy, neutron scattering and physisorption approach. *International Journal of Coal Geology*, 249:103880.
- Devoie, E. G., Gruber, S., and McKenzie, J. M. (2022). A repository of measured soil freezing characteristic curves: 1921 to 2021. *Earth System Science Data*, 14(7):3365–3377.
- Dillon, H. B. and Andersland, O. B. (1966). Predicting unfrozen water contents in frozen soils. *Canadian Geotechnical Journal*, 3(2):53–60.
- Ding, W., Liu, X., Hu, F., Zhu, H., Luo, Y., Li, S., and Li, H. (2019). How the particle interaction forces determine soil water infiltration: Specific ion effects. *Journal of Hydrology*, 568:492–500.
- Dobson, M. C., Ulaby, F. T., Hallikainen, M. T., and El-rayes, M. A. (1985). Microwave dielectric behavior of wet soil-part ii: Dielectric mixing models. *IEEE Transactions on Geoscience and Remote Sensing*, GE-23(1):35–46.
- Dyck, M., Miyamoto, T., Iwata, Y., and Kameyama, K. (2019). Bound water, phase configuration, and dielectric damping effects on tdr-measured apparent permittivity. *Vadose Zone Journal*, 18(1):1–14.
- Ellingson, S. W. (2020). Electromagnetics, Volume 2. *VT Publishing*.

- Evans, S. (1965). Dielectric properties of ice and snow—a review. *Journal of Glaciology*, 5(42):773–792.
- Fisher, D. A., Lacelle, D., and Pollard, W. (2019). A model of unfrozen water content and its transport in icy permafrost soils: Effects on ground ice content and permafrost stability. *Permafrost and Periglacial Processes*, 31(1):184–199.
- Fukuta, N. and Mason, B. (1963). Epitaxial growth of ice on organic crystals. *Journal of Physics and Chemistry of Solids*, 24(6):715–718.
- Fussmann, K. E., Schwarzmüller, F., Brose, U., Jousset, A., and Rall, B. C. (2014). Ecological stability in response to warming. *Nature Climate Change*, 4(3):206–210.
- Ge, S., McKenzie, J., Voss, C., and Wu, Q. (2011). Exchange of groundwater and surface-water mediated by permafrost response to seasonal and long term air temperature variation: Groundwater and permafrost. *Geophysical Research Letters*, 38(14).
- Grimm, U. (2015). Aperiodic crystals and beyond. *Acta Crystallographica B* 71 (2015) 258-274.
- Groenendyk, D., Ferré, T., Thorp, K., and Rice, A. (2015). Hydrologic-process-based soil texture classifications for improved visualization of landscape function. *PloS one*, 10:e0131299.
- He, H., Dyck, M., Zhao, Y., Si, B., Jin, H., Zhang, T., Lv, J., and Wang, J. (2016). Evaluation of five composite dielectric mixing models for understanding relationships between effective permittivity and unfrozen water content. *Cold Regions Science and Technology*, 130:33–42.
- Head, R. B. (1961). Steroids as ice nucleators. *Nature*, 191(4793):1058–1059.

- Hermann, A., Ashcroft, N. W., and Hoffmann, R. (2012). High pressure ices. *Proceedings of the National Academy of Sciences*, 109(3):745–750.
- Indraratna, B., Singh, M., Nguyen, T. T., Leroueil, S., Abeywickrama, A., Kelly, R., and Neville, T. (2020). Laboratory study on subgrade fluidization under undrained cyclic triaxial loading. *Canadian Geotechnical Journal*, 57(11):1767–1779.
- Jin, H., Huang, Y., Bense, V. F., Ma, Q., Marchenko, S. S., Shepelev, V. V., Hu, Y., Liang, S., Spektor, V. V., Jin, X., Li, X., and Li, X. (2022). Permafrost degradation and its hydrogeological impacts. *Water*, 14(3).
- Jin, X., Yang, W., Gao, X., and Li, Z. (2020). Analysis and modeling of the complex dielectric constant of bound water with application in soil microwave remote sensing. *Remote Sensing*, 12(21).
- Jin, X.-Y., Jin, H.-J., Iwahana, G., Marchenko, S. S., Luo, D.-L., Li, X.-Y., and Liang, S.-H. (2021). Impacts of climate-induced permafrost degradation on vegetation: A review. *Advances in Climate Change Research*, 12(1):29–47. Including special topic on degrading permafrost and its impacts.
- Joe Wolfe, G. B. and Koster, K. L. (2002). What is 'unfreezable water', how unfreezeable is it, and how much is there? *Cryo Letters*, 23(3):157–166.
- Jones, S. B. (2002). Wintdr. *University of Utah*.
- Kleinberg, R. and Griffin, D. (2005). Nmr measurements of permafrost: unfrozen water assay, pore-scale distribution of ice, and hydraulic permeability of sediments. *Cold Regions Science and Technology*, 42(1):63–77.

- Koopmans, R. W. R. and Miller, R. D. (1966). Soil freezing and soil water characteristic curves. *Soil Science Society of America Journal*, 30(6):680–685.
- Kozlowski, T. (2007). A semi-empirical model for phase composition of water in clay–water systems. *Cold Regions Science and Technology*, 49(3):226–236.
- Ktigel-Knabner, I. (1997). ^{13}C and ^{15}N nmr spectroscopy as a tool in soil organic matter studies. *Elsevier*.
- Kuehn, R., Kilian, R., Lang, D., Morales, L. G., Grendal, O. G., and Stipp, M. (2024). Clay alignment takes place during early stages of sedimentation. *Communications Earth & Environment*, 5(1):696.
- Kurylyk, B. L. and Watanabe, K. (2013). The mathematical representation of freezing and thawing processes in variably-saturated, non-deformable soils. *Advances in Water Resources*, 60:160–177.
- Leelamanie, D. A. L. and Karube, J. (2009). Effects of hydrophobic and hydrophilic organic matter on the water repellency of model sandy soils. *Soil Science and Plant Nutrition*, 55(4):462–467.
- Lei, P., Young, M. W., Seymour, J. D., Stillman, D. E., Primm, K., Sizemore, H. G., Rempel, A. W., and Codd, S. L. (2022). NMR characterization of unfrozen brine vein distribution and structure in model packed beds. *Cold Regions Science and Technology*, 199:103572.
- Lemieux, J., Frampton, A., and Fortier, P. (2024). Recent advances (2018–2023) and research opportunities in the study of groundwater in cold regions. *Permafrost and Periglacial Processes*, 36(1):93–109.

- Li, X., Zheng, S.-F., Wang, M., and Liu, A.-Q. (2023). The prediction of the soil freezing characteristic curve using the soil water characteristic curve. *Cold Regions Science and Technology*, 212:103880.
- Li, Z., Yang, G., Wang, B., and Wang, J. (2025). Study on unfrosted water content and strength characteristics of saturated sandstone during thawing process. *Scientific Reports*, 15(1).
- Li, Z., Zhou, Z., Dai, Y., and Dai, B. (2019). Contaminant transport in a largely-deformed aquitard affected by delayed drainage. *Journal of Contaminant Hydrology*, 221:118–126.
- Lijith, K., Sharma, V., and Singh, D. N. (2021). A methodology to establish freezing characteristics of partially saturated sands. *Cold Regions Science and Technology*, 189:103333.
- Liu, L., Sletten, R. S., Hallet, B., and Waddington, E. D. (2018). Thermal regime and properties of soils and ice-rich permafrost in beacon valley, antarctica. *Journal of Geophysical Research: Earth Surface*, 123(8):1797–1810.
- Liu, X., Feng, B., Tian, R., Li, R., Tang, Y., Wu, L., Ding, W., and Li, H. (2020). Electrical double layer interactions between soil colloidal particles: Polarization of water molecule and counterion. *Geoderma*, 380:114693.
- Mady, A. Y. and Shein, E. V. (2020). Assessment of pore space changes during drying and wetting cycles in hysteresis of soil water retention curve in russia using x-ray computed tomography. *Geoderma Regional*, 21:e00259.
- Maeda, N. (2021). Brief overview of ice nucleation. *Molecules*, 26(2).
- Malmberg, C. G. and Maryott, A. A. (1956). Dielectric constant of water from 0 to 100 c. *Journal of research of the National Bureau of Standards*, 56:1.

- Mauritz, K. (2014). Dielectric spectroscopy. *University of Southern Mississippi*.
- Mayergoyz, I. and Friedman, G. (1988). Generalized preisach model of hysteresis. *IEEE Transactions on Magnetics*, 24(1):212–217.
- McCarthy, A., Chelle-Michou, C., Blundy, J. D., Dorais, M. J., van der Zwan, F. M., and Peate, D. W. (2023). The effect of variations in cooling rates on mineral compositions in mid-ocean ridge basalts. *Chemical Geology*, 625:121415.
- McKenzie, J., Voss, C. I., and Siegel, D. I. (2007). Groundwater flow with energy transport and water–ice phase change: Numerical simulations, benchmarks, and application to freezing in peat bogs. *Advances in Water Resources*, 30(4):966–983.
- METER (2025a). 5tm documentation.
- METER (2025b). The researchers complete guide to soil moisture.
- Minasny, B. and McBratney, A. B. (2017). Limited effect of organic matter on soil available water capacity. *European Journal of Soil Science*, 69(1):39–47.
- Mualem, Y. (1973). Modified approach to capillary hysteresis based on a similarity hypothesis. *Water Resources Research*, 9(5):1324–1331.
- Nambu, K., van Hees, P., Jones, D., Vinogradoff, S., and Lundström, U. (2008). Composition of organic solutes and respiration in soils derived from alkaline and non-alkaline parent materials. *Geoderma*, 144(3):468–477.
- NRCA (1988). Glossary of permafrost and related ground-ice terms. *National Research Council of Canada*.

- Obu, J. (2021). How much of the earth's surface is underlain by permafrost? *Journal of Geophysical Research: Earth Surface*, 126(5):e2021JF006123. e2021JF006123 2021JF006123.
- Olphen, H. V. (1964). An introduction to clay colloid chemistry. *J. Pharm. Sci.*, 53(2):230.
- Outcalt, S. I., Nelson, F. E., and Hinkel, K. M. (1990). The zero-curtain effect: Heat and mass transfer across an isothermal region in freezing soil. *Water Resources Research*, 26(7):1509–1516.
- Patton, A. I., Rathburn, S. L., Capps, D. M., McGrath, D., and Brown, R. A. (2021). Ongoing landslide deformation in thawing permafrost. *Geophysical Research Letters*, 48(16).
- Polder, D. and van Santeen, J. (1946). The effective permeability of mixtures of solids. *Physica*, 12(5):257–271.
- Pummer, B. G., Budke, C., Augustin-Bauditz, S., Niedermeier, D., Felgitsch, L., Kampf, C. J., Huber, R. G., Liedl, K. R., Loerting, T., Moschen, T., Schauperl, M., Tollinger, M., Morris, C. E., Wex, H., Grothe, H., Pöschl, U., Koop, T., and Fröhlich-Nowoisky, J. (2015). Ice nucleation by water-soluble macromolecules. *Atmospheric Chemistry and Physics*, 15(8):4077–4091.
- Ramage, J., Jungsberg, L., Wang, S., Westermann, S., Lantuit, H., and Heleniak, T. (2021). Population living on permafrost in the arctic. *Population and Environment*, 43(1):22–38.
- Rantanen, M., Karpechko, A. Y., Lippinen, A., Nordling, K., Hyvärinen, O., Ruosteenoja, K., Vihma, T., and Laaksonen, A. (2022). The arctic has warmed nearly four times faster than the globe since 1979. *Communications Earth & Environment*, 3(1):168.

- Rayssi, C., El.Kossi, S., Dhahri, J., and Khirouni, K. (2018). Frequency and temperature-dependence of dielectric permittivity and electric modulus studies of the solid solution $\text{ca}0.85\text{er}0.1\text{ti}1\text{xco}4\text{x}/3\text{o}3$ (0×0.1). *RSC Advances*, 8(31):17139–17150.
- Resurreccion, A. C., Moldrup, P., Tuller, M., Ferré, T. P. A., Kawamoto, K., Komatsu, T., and de Jonge, L. W. (2011). Relationship between specific surface area and the dry end of the water retention curve for soils with varying clay and organic carbon contents. *Water Resources Research*, 47(6).
- Romanovsky, V. E., Smith, S. L., and Christiansen, H. H. (2010). Permafrost thermal state in the polar northern hemisphere during the international polar year 2007–2009: a synthesis. *Permafrost and Periglacial Processes*, 21(2):106–116.
- Sae-Lim, J. N., Konecky, B. L., Morrill, C., Michelutti, N., Grooms, C., and Smol, J. P. (2025). Lake energy balance response to 21st century warming in the tropical high andes. *Global and Planetary Change*, 248:104741.
- Sami, S., Alessandri, R., W. Wijaya, J. B., Grünewald, F., de Vries, A. H., Marrink, S. J., Broer, R., and Havenith, R. W. A. (2022). Strategies for enhancing the dielectric constant of organic materials. *The Journal of Physical Chemistry C*, 126(45):19462–19469.
- Samset, B. H., Zhou, C., Fuglestvedt, J. S., Lund, M. T., Marotzke, J., and Zelinka, M. D. (2023). Steady global surface warming from 1973 to 2022 but increased warming rate after 1990. *Communications Earth & Environment*, 4(1).
- Sarker, P. C., Guo, Y., Lu, H. Y., and Zhu, J. G. (2020). A generalized inverse Preisach dynamic hysteresis model of Fe-based amorphous magnetic materials. *Journal of Magnetism and Magnetic Materials*, 514:167290.

- Shang, J., Lo, K., and Quigley, R. (1994). Quantitative determination of potential distribution in stern–gouy double-layer model. *Canadian Geotechnical Journal*, 31(5):624–636.
- Shusherina, E. P., Bobkov, Y. P., and National Research Council Of Canada. Division Of Building Research (1978). Effect of moisture content on frozen ground strength.
- Sihvola, A. (2000). Mixing rules with complex dielectric coefficients. *Subsurface Sensing Technologies and Applications*, 1(4):393–415.
- Sihvola, A. and Alanen, E. (1991). Study of mixing formulae in the complex plane. *Transactions on Geoscience and Remote Sensing*, 29.
- Sihvola, A. and Kong, J. (1988). Effective permittivity of dielectric mixtures. *IEEE Transactions on Geoscience and Remote Sensing*, 26(4):420–429.
- Sivarajah, B., Simmatis, B., Favot, E. J., Palmer, M. J., and Smol, J. P. (2021). Eutrophication and climatic changes lead to unprecedented cyanobacterial blooms in a canadian sub-arctic landscape. *Harmful Algae*, 105:102036.
- Smith, M. W. and Tice, A. R. (1988). Measurement of the unfrozen water content of soils comparison of nmr and tdr methods. *Cold Regions Research and Engineering Lab, Hanover NH*.
- Sun, T., Gao, X., Liao, Y., and Feng, W. (2021). Experimental study on adfreezing strength at the interface between silt and concrete. *Cold Regions Science and Technology*, 190:103346.
- Suzuki, S. (2004). Dependence of unfrozen water content in unsaturated frozen clay soil on initial soil moisture content. *Soil Science and Plant Nutrition*, 50(4):603–606.

- Tian, H., Wei, C., Wei, H., and Zhou, J. (2014). Freezing and thawing characteristics of frozen soils: Bound water content and hysteresis phenomenon. *Cold Regions Science and Technology*, 103:74–81.
- Topp, G. C., Davis, J. L., and Annan, A. P. (1980). Electromagnetic determination of soil water content: Measurements in coaxial transmission lines. *Water Resour. Res.*, 16(3):574–582.
- USEPA (2024). Climate change indicators: Permafrost. *United States Environmental Protection Agency*.
- USGS (2016). Quality of ground water. U.S. Geological Survey. <https://pubs.usgs.gov/gip/gw/quality.html>.
- Verwey, E. J. W. (1947). Theory of the stability of lyophobic colloids. *The Journal of Physical and Colloid Chemistry*, 51(3):631–636.
- Vu, Q. H., Pereira, J.-M., and Tang, A. M. (2022). Effect of fines content on soil freezing characteristic curve of sandy soils. *Acta Geotechnica*, 17(11):4921–4933.
- Walvoord, M. A. and Kurylyk, B. L. (2016). Hydrologic impacts of thawing permafrost—a review. *Vadose Zone Journal*, 15(6):vzj2016.01.0010.
- Wan, Z., Bian, X., and Chen, Y. (2022). Mud pumping in high-speed railway: in-situ soil core test and full-scale model testing. *Railway Engineering Science*, 30(3):289–303.
- Wang, L., Wang, L., Li, Y., and Wang, J. (2023). A century-long analysis of global warming and earth temperature using a random walk with drift approach. *Decision Analytics Journal*, 7:100237.

- Wang, L., Wang, X., Han, J., Wang, C., Zhang, C., and Huo, Z. (2024). A novel generalized clapeyron equation-based model for capturing the soil freezing characteristics curve of saline soil: Validation by small sample lab and field experiments. *Water*, 16(5).
- Warren, J. and Spiers, G. (2021). Soil mineralogy. *University of Guelph and Laurentian University*. <https://www.saskoer.ca/soilscience/chapter/soil-mineralogy/>.
- Watanabe, K. and Osada, Y. (2017). Simultaneous measurement of unfrozen water content and hydraulic conductivity of partially frozen soil near 0°C. *Cold Regions Science and Technology*, 142:79–84.
- Wei, C. and Dewoolkar, M. M. (2006). Formulation of capillary hysteresis with internal state variables. *Water Resources Research*, 42(7).
- Williams, P. J. (1964). Unfrozen water content of frozen soils and soil moisture suction. *Géotechnique*, 14(3):231–246.
- Wolfe, J. (2025). What is 'unfreezable water'? is it the same as bound water or water of hydration? <https://www.phys.unsw.edu.au/jw/unfreezable.html>.
- Wu, J. Y. (1977). Heat and mass transfer in freezing unsaturated soil. *PhD*.
- Wu, Z., Wu, S., Hou, Y., Zhang, M., Liang, J., and Cai, C. (2024). Contrast of hydraulic conductivity induces transport of combined pollutants in high- and low-permeability systems. *Ecotoxicology and Environmental Safety*, 287:117297.
- Yang, X., Liu, J., and Koster, L. J. A. (2024). The exceptionally high dielectric constant of doped organic semiconductors. *Advanced Electronic Materials*, 11(3).

Zou, Y., Jiang, H., Wang, E., Liu, X., and Du, S. (2023). Variation and prediction of unfrozen water content in different soils at extremely low temperature conditions. *Journal of Hydrology*, 624:129900.

Appendix A

Time Program Analysis and Temperature Correction

In order to create an optimal Time Program for the climate chamber to obtain the best possible data points to populate an SFCC, diagrams such as Figure A.1 were created from trial runs and examined to assess whether the temperature steps were adequate to achieve thermal equilibrium in the system (Figure A.1).

The goal is to assess whether a) the system reaches equilibrium at every temperature step and b) if the scope of the Time Program properly captures the Freeze-Thaw process. The STM capacitance sensor makes two measurements: the blue ([Temperature sensor reading](#)) and the red ([raw dielectric permittivity](#)) in each timestep. The inner temperature of the system varies not only because of the change of temperature within the climate chamber ([green](#) data points), but also because of the release of latent heat as ice forms. This behavior is most apparent in the rise and 0°C plateau behavior of the sensor readings which follow the first nucleation of ice around -3°C . The dielectric permittivity also varies with ice content: it plummets whenever ice forms.

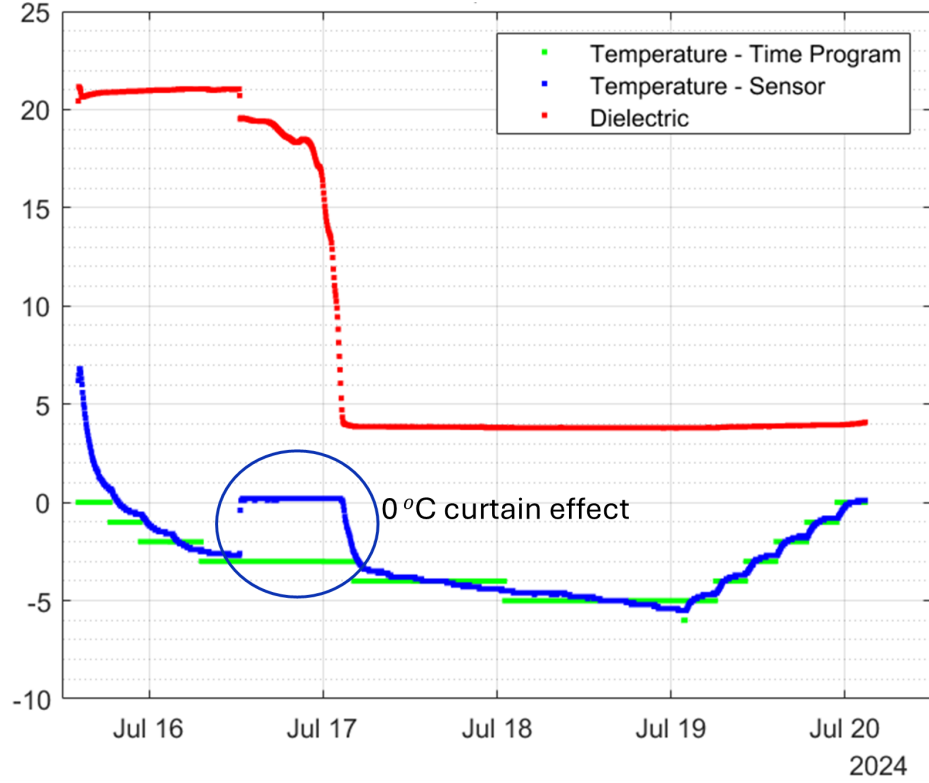


Figure A.1: Experimental Time Program for a fully saturated bucket of 20/30 sand. Notice the significant time (x axis) and temperature (y axis) lag between the blue (Temperature sensor reading) and green (Time Program) data points showing, respectively, the heat propagation into the bucket and the response of the sensor. The red (raw dielectric permittivity) data points are to be used as a proxy to illustrate the progressive formation of ice in the system.

Once the dielectric permittivity plumets and plateaus, all of the free water available for freezing is expected to have been turned into ice. Another point of interest lies in the intermediate steps in the freezing limb between -3 and -5 $^{\circ}\text{C}$ where the blue (Temperature sensor reading) can be seen struggling to properly plateau despite being given ample time to equilibrate and even overshooting the time program temperature. We believe this to be an artifact of both a) the resolution of the sensor ($\pm 0.1^{\circ}\text{C}$) being close to the amplitude of our Temperature step, namely 0.2°C , and b) latent heat release from ice nucleation as

the system attempts to reach equilibrium. It is possible to assess that Figure A.1 requires longer temperature plateaus because the inner temperature readings from the sensor never stabilize, meaning that the system never reaches equilibrium with its surroundings.

Comparing the sensor's temperature to the measured chamber temperature is also insightful to correct for systematic error. Thermodynamically speaking, if given ample time to reach equilibrium, the samples within the climate chamber should always equilibrate to the temperature at which the chamber is set. Accordingly, at equilibrium, any consistent offset of temperature can be attributed to a systematic error in the sensor's temperature functionality. For example, figure A.2 shows one dataset which has consistent offset.

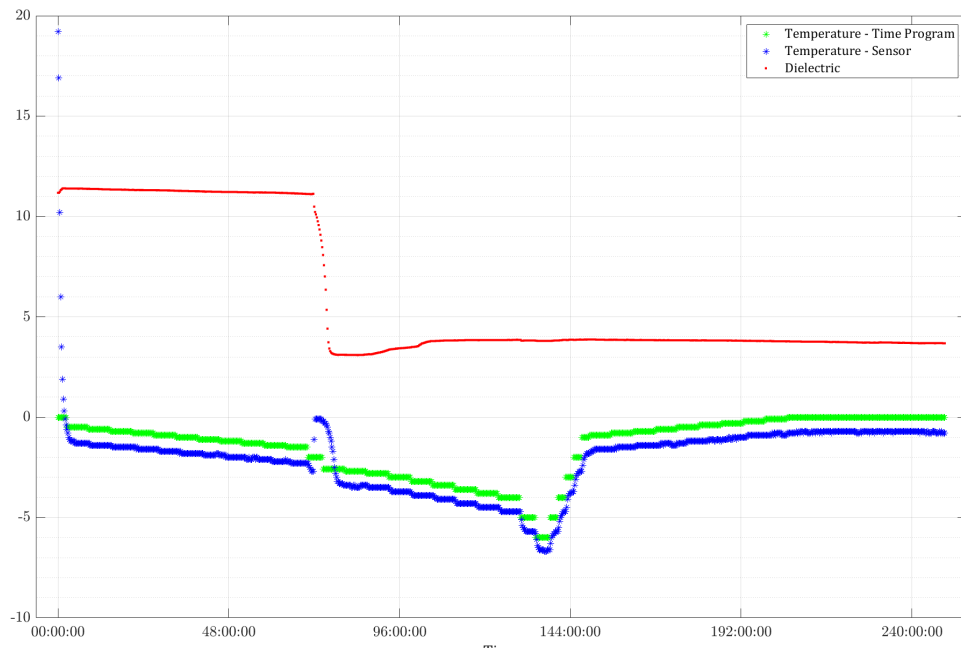


Figure A.2: Time Program for a fully saturated 800 ml beaker of silica sand. Notice the consistent offset from the sensor's temperature (in blue) and the climate chamber's time program (in green).

In order to assess the correct correction factor to apply to the sensor's temperature, a simple residuals analysis can be made similarly to the one shown in Figure A.3.

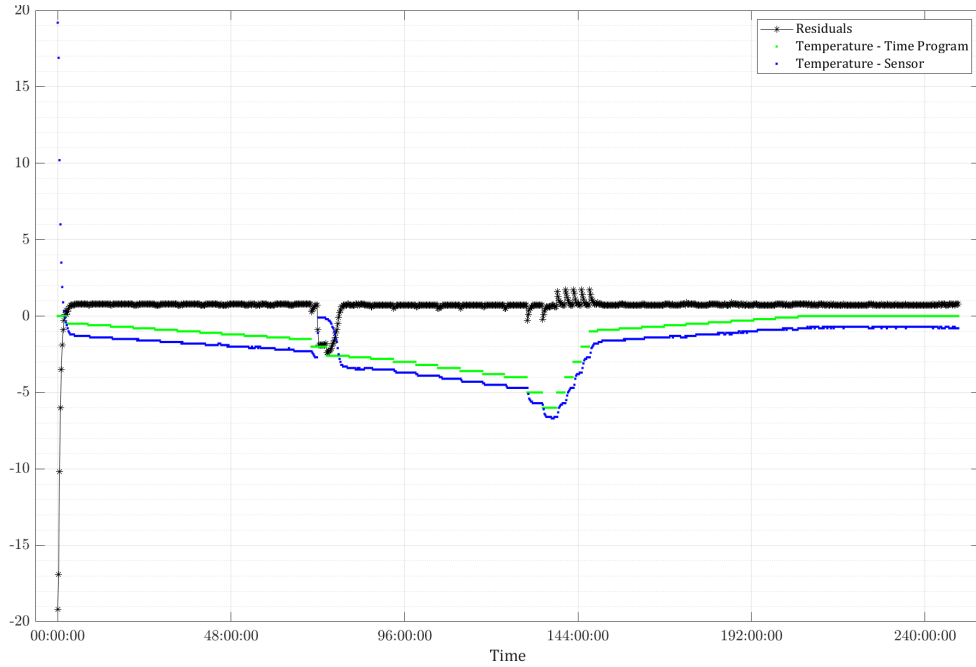


Figure A.3: Residuals (in black) of the sensor's Temperature VS the Time Program for a fully saturated 800 ml beaker of silica sand.

There is an expected lack of equilibrium in later thawing phases because a major phase change of ice to water is expected to require a lot of latent heat. The residuals here help pinpoint the appropriate correction to the sensor's temperature without stamping out the impact of latent heat during major phase change events resulting in non-equilibrium behaviour. Upon correction, the data are shown in Figure A.4.

The only statistically significant data points are ones at which the system is in thermodynamic equilibrium. That is, where the Temperature recorded in the sample is stable and in

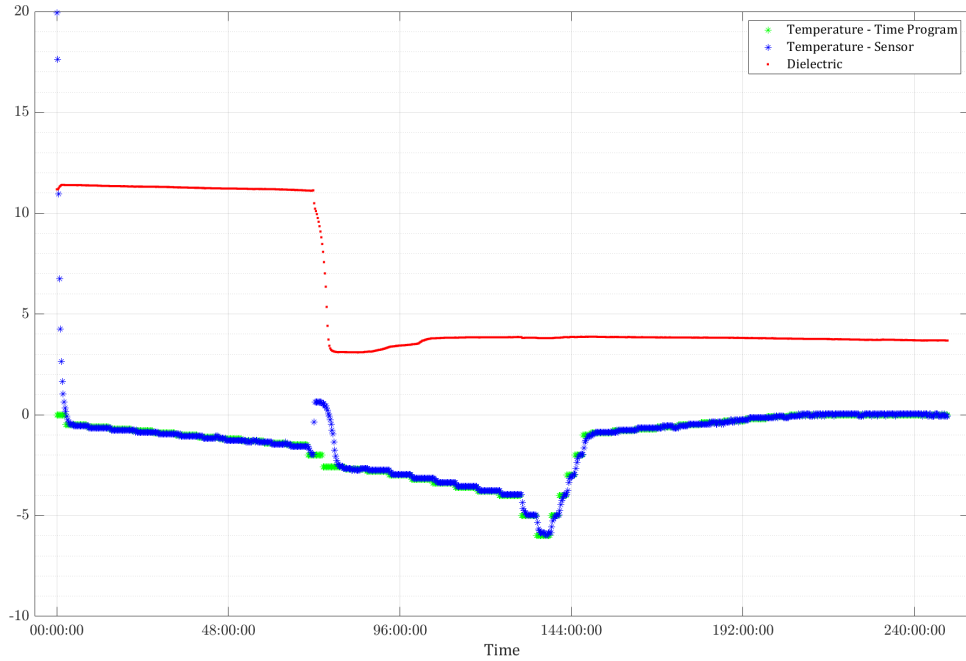


Figure A.4: Corrected Temperature VS the Time Program for a fully saturated 800 ml beaker of silica sand.

line with the Climate Chamber's current Temperature. The same residual study test (Figure A.5) between the now Systematic Error Corrected Sensor Temperature and the Climate Chamber Temperature can be used to remove data points that are not in Equilibrium (A.6). In this specific case, the data removed mostly lies in the early phase of the freezing limb when the climate chamber was adjusting from room temperature to -6°C and in the later stages when thawing occurred.

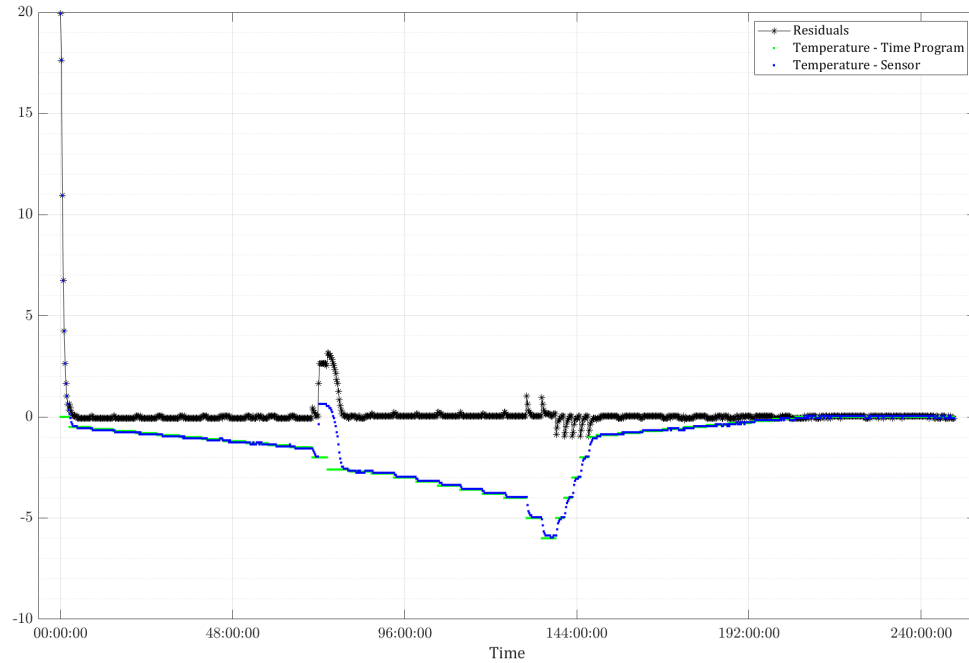


Figure A.5: Residual study for Equilibrium points selection.

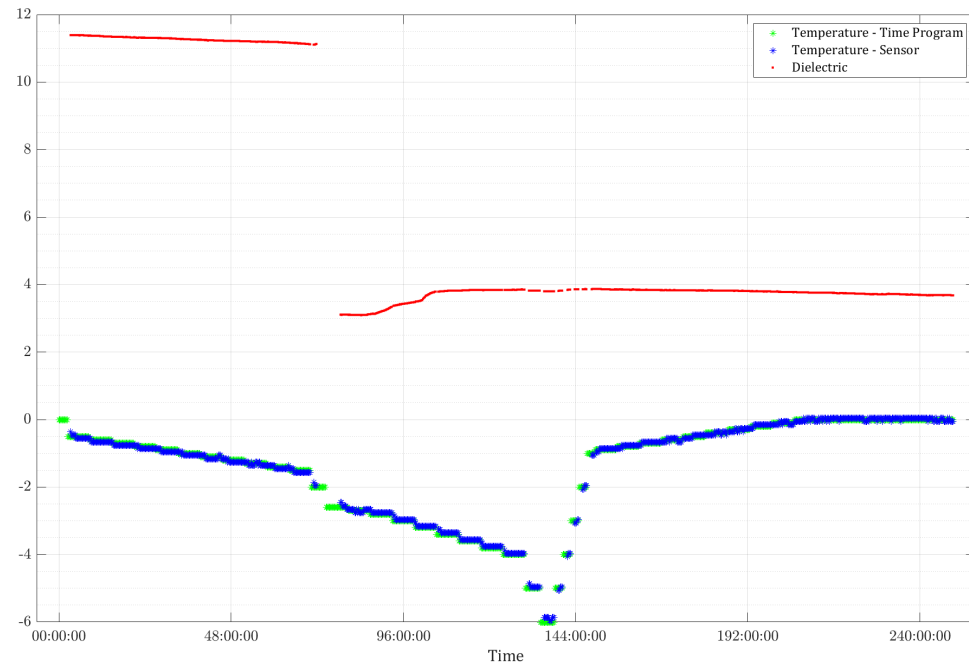


Figure A.6: Final Data set of Equilibrium Points to be converted with the Conversion Curve.

Appendix B

Solver

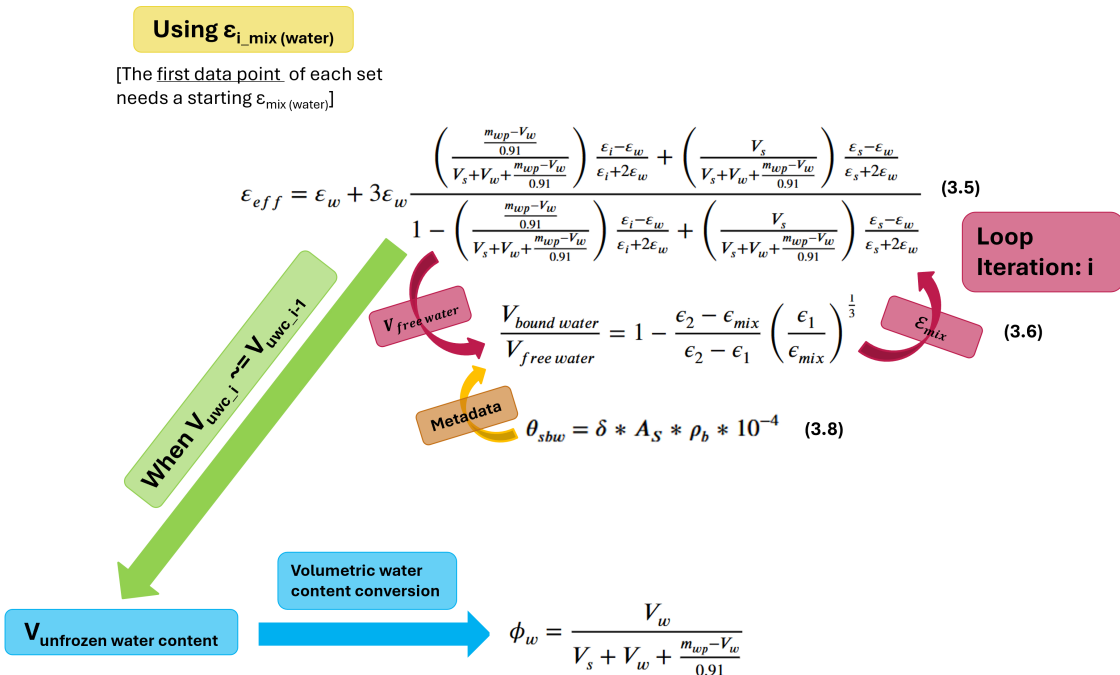


Figure B.1: Schematic representation of the iterative solver for the system of equations describing the mixing model developed in this study. The system of equations comprises Eq. 3.5, Eq. 3.6 and Eq. 3.8.

Figure B.1 represents the iterative algorithm used to solve the system of equations. Metadata parameters (δ , A_s and ρ_b) are inputted into the strongly bounded water characterization

Port Number	1	2	3	4	5	6
Soil Type	Garden soil - Higher Org. Content A	Garden soil - Lower Org. Content	Garden soil - Higher Org. Content B	20/30 Sand A	20/30 Sand B	Silica Flour
Water Type	Tap	Tap	Tap	DI	DI	DI
Volume of Water for full saturation (in ml)	266.53	248.76	252.66	224.52	233.26	204.71
Porosity ϕ	0.4761	0.3724	0.4413	0.3601	0.3741	0.4290
Specific Surface Area A_s (in m^2/g)	80	80	80	30	30	120
Bulk Density ρ_b (in g/cm^3)	1.40	1.40	1.40	1.60	1.60	1.28
Strongly Bound Water Layer Thickness δ (in Å)	5	5	5	5	5	5

Table B.1: : Input parameters for the 6 soils used for Freeze-Thaw experiments. These are required to run the model presented in Figure B.1.

(eq. 3.8) which yield the $V_{bound\ water}$ variable of the adaptive dielectric of water phase (eq. 3.6). The fully saturated 3 phase mixing model (eq. 3.5) is then solved for the first data point with a starting $\epsilon_{mix\ water}$ this usually will be a room temperature measurement ($>0^\circ C$) as the sample is readied to be slowly frozen. For instance, the starting $\epsilon_{mix\ water}$ at $>0^\circ C$ for all datasets represented in Figure 3.5 was 79.55 with an assigned strongly bounded water dielectric of 9, a free water dielectric of 87.40 used in the adaptive dielectric of water phase model (eq. 3.6, see Figure 3.3) (Malmberg and Maryott, 1956; Jin et al., 2020).

The iterative solver algorithm works as follow: Equation 3.5 is solved and a $V_{free\ water}$ is found for the given $\epsilon_{mix\ water}$ used in this loop. Equation 3.6 is then solved using $V_{free\ water}$ and a $\epsilon_{mix\ water}$ is output. If the $\epsilon_{mix\ water}$ output is close enough to the one initially used to solve equation 3.5, the loop ends and the $V_{free\ water}$ found in the iteration is the $V_{unfrozen\ water\ content}$ for the data point. Otherwise, the new $\epsilon_{mix\ water}$ is sent back to Equation 3.5 and the loop continues. Once the loop is finished, $V_{unfrozen\ water\ content}$ is transformed into $\theta_{unfrozen\ water\ content}$. To start the same process for the next data point, the appropriate $\epsilon_{mix\ water}$ (the one used to

solve the system) from the previously solved loop can be used as the starting point for the new loop. This comes from the principle that it should be quite close to the correct $\varepsilon_{mix\ water}$ since the T from one data point to the next is similar, as is their unfrozen water content.

Appendix C

Raw Dielectric Permittivity Data Example

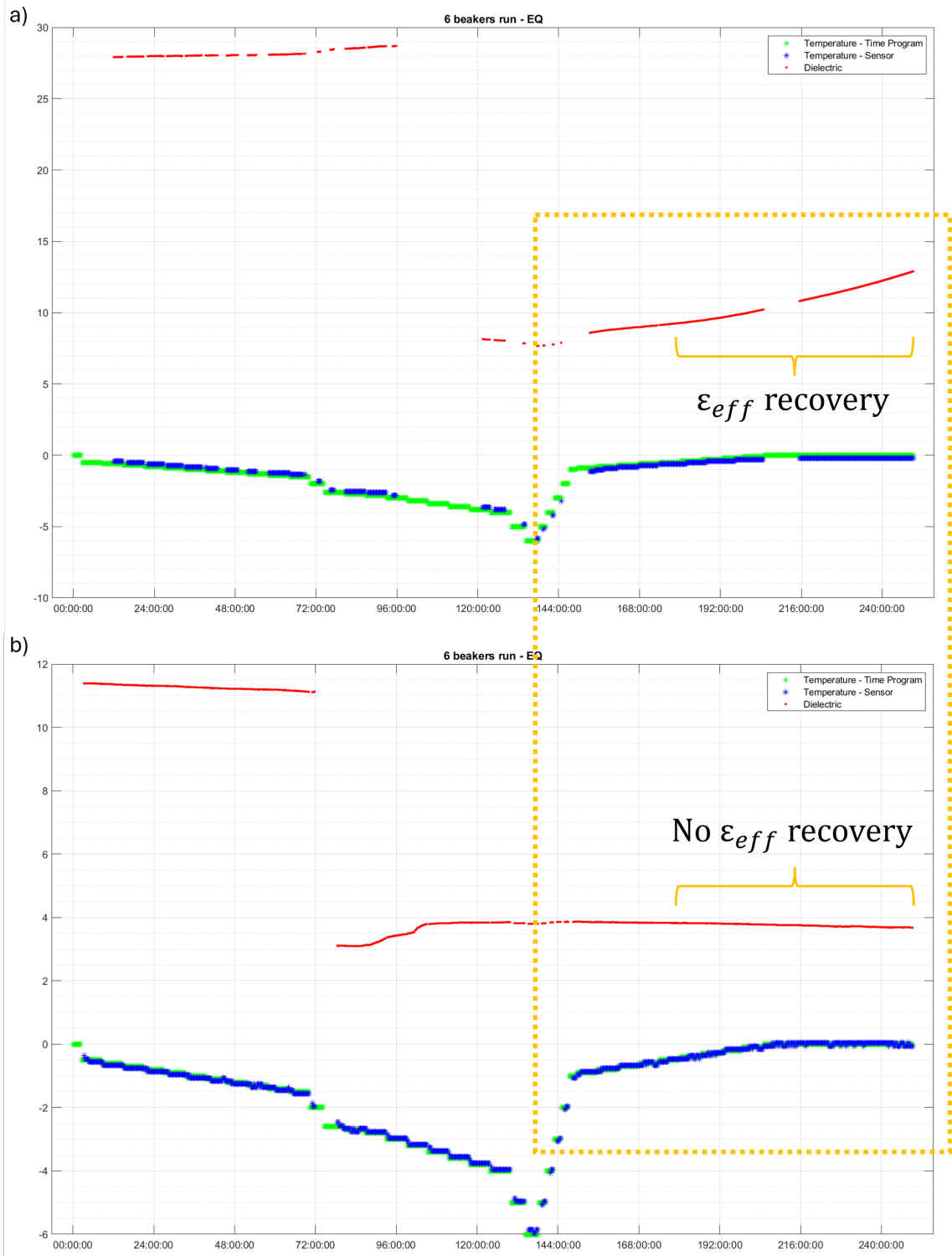


Figure C.1: Full Freeze-Thaw cycle raw dielectric plots for Garden Soil – Higher Org. Content A (a) and Silica Flour (b). Notice that, in the thawing limb, the dielectric doesn't recover/increase despite being given ample time to equilibrate at 0°C (in the orange dotted box). This is associated to a stable ice phase for the silica flour, but not the Garden soil, resulting in a dielectric increase for a) but not b).